

# Resonance damping of the terahertz-frequency transverse acoustic phonon in the relaxor ferroelectric $\text{KTa}_{1-x}\text{Nb}_x\text{O}_3$

J. Toulouse,<sup>1,\*</sup> E. Iolin,<sup>1,2,†</sup> B. Hennion,<sup>3</sup> D. Petitgrand,<sup>3</sup> and R. Erwin<sup>4</sup>

<sup>1</sup>*Physics Department, Lehigh University, Bethlehem, Pennsylvania 18015, USA*

<sup>2</sup>*Latvian Academy of Science, Riga, Latvia*

<sup>3</sup>*Laboratoire Leon Brillouin, CEA, Saclay 91400, France*

<sup>4</sup>*National Center for Neutron Research, NIST, Gaithersburg, Maryland 20899, USA*

(Received 4 August 2016; published 30 December 2016)

The damping ( $\Gamma_a$ ) of the transverse acoustic (TA) phonon in single crystals of the relaxor  $\text{KTa}_{1-x}\text{Nb}_x\text{O}_3$  with  $x = 0.15\text{--}0.17$  was studied by means of high resolution inelastic cold neutron scattering near the (200) Brillouin Zone (BZ) point where diffuse scattering is absent, although it is present near (110). In a wide range of temperatures centered on the phase transition,  $T = 195\text{ K} \div 108\text{ K}$ , the TA phonon width (damping) exhibits a step increase around momentum  $q = 0.07$ , goes through a shallow maximum at  $q = 0.09\text{--}0.12$ , and remains high above and up to the highest momentum studied of  $q = 0.16$ . These experimental results are explained in terms of a resonant interaction between the TA phonon and the collective or correlated reorientation through tunneling of the off-center  $\text{Nb}^{+5}$  ions. The observed TA damping is successfully reproduced in a simple model that includes an interaction between the TA phonon and a dispersionless localized mode (LM) with frequency  $\omega_L$  and damping  $\Gamma_L$  ( $\Gamma_L < \omega_L$ ), itself coupled to the transverse optic (TO) mode. Maximum damping of the TA phonon occurs when its frequency is  $\omega_a \approx \omega_L$ . The values of  $\omega_L$  and  $\Gamma_L$  are moderately dependent on temperature, but the oscillator strength,  $M^2$ , of the resonant damping exhibits a strong maximum in the range  $T \sim 120\text{ K} \div 150\text{ K}$  in which neutron diffuse scattering near the (110) BZ point is also maximum and the dielectric susceptibility exhibits the relaxor behavior. The maximum value of  $M$  appears to be due to the increasing number of polar nanodomains. In support of the proposed model, the observed value of  $\omega_L \approx 0.7\text{ THz}$  is found to be similar to the estimate previously obtained by Girshberg and Yacoby [J. Phys.: Condens. Matter **24**, 015901 (2012)]. Alternatively, the TA phonon damping can be successfully fitted in the framework of an empirical Havriliak-Negami (HN) relaxation model that includes a strong resonancelike transient contribution.

DOI: [10.1103/PhysRevB.94.214116](https://doi.org/10.1103/PhysRevB.94.214116)

## I. INTRODUCTION

The KTN is a member of the family of relaxor ferroelectrics, a now well recognized subgroup of highly polarizable compounds with substitutional disorder and off-center ions displaced from their high symmetry lattice site (see review and recent results [1]). Other well-known and extensively studied systems of the same family are the lead compounds  $\text{PbMg}_{1/3}\text{Nb}_{2/3}\text{O}_3$  (PMN) and  $\text{PbZn}_{1/3}\text{Nb}_{2/3}\text{O}_3$  (PZN). With decreasing temperature, correlations develop between the dipoles introduced by the off-center ions, leading to the formation of polar nanoregions (PNRs) below a temperature known as Burns temperature,  $T_d$ . At a still lower temperature,  $T^* < T_d$ , the dielectric susceptibility begins to exhibit the characteristic frequency dispersion displayed by relaxor ferroelectrics. This suggests a distinction between quasistatic PNRs, resulting from dynamical polar correlations, and polar nanodomains (PNDs) [2] when these correlations become static or long lived, resulting in local distortions evidenced by the elastic diffuse scattering (DS) shown below. The existence of quasistatic PNRs in the intermediate temperature range  $T^* < T < T_d$  has been recognized for a long time and was initially thought confirmed by neutron DS. In the past few years, however, it has been found that the DS observed in this intermediate temperature range corresponds to quasielastic

scattering by low energy phonons [1]. True elastic DS appears only at a lower temperature than Burns temperature,  $T_{dr} < T_d$ , where  $T_{dr}$  appears to coincide with the temperature  $T^*$  at which the static PNDs appear. In the case of PMN, for example,  $T_d = 620\text{ K}$ , but  $T_{dr} = 420 \pm 20\text{ K}$ , which is indeed very close to  $T^* \approx 400\text{ K}$  [2]. Eventually, long range (LR) ferroelectric order develops at a lower Curie temperature,  $T_c < T^*$ . These recent findings suggest that one should reexamine the original meaning of Burns temperature,  $T_d$ , and the development of the local polar order. What appears to be well established at least is the presence of precursors in the dynamical pair correlation in the range  $T^* < T < T_d$  [1]. New data concerning the genesis of PNRs have recently been reported by Manley *et al.* [3]. These authors have measured inelastic neutron scattering in a single crystal  $\text{PMN-30\%PbTiO}_3$  (PMN-PT) and have found additional intensity between the transverse acoustic (TA) and transverse optic (TO) branches,  $E_{\text{TA}}(q) < E_{\text{RM}}(q) < E_{\text{TO}}(q)$ , exhibiting little dispersion and probably due to phonon localized modes (LMs). They have suggested that the interaction between the lattice TO phonon and a low dispersion LM is the driving force leading to the appearance of PNRs. However, Gehring *et al.* [4] have recently shown that the peak observed in the data [3] is spurious and most likely results from a simple double scattering process involving a longitudinal acoustic (LA) mode and strong elastic Bragg scattering at the (2, -4, 0) Brillouin Zone (BZ) point.

Diffuse scattering (DS) in relaxors can, in fact, exhibit unusual features, and its connection to the damping of the TO and TA phonons is still unclear. (i) In PMN, Hirota *et al.*

\*jt02@lehigh.edu

†eiolin@netzero.net

reported strong DS near the (110) BZ point but very weak or almost absent near (200) [5]. They explained their results by proposing that DS is not necessarily due to a condensed soft TO mode but can also be due to a *collective shift*  $\delta$  of *all the atoms within a PNR* along the local polar direction, which should certainly have an effect on the TA phonon. (ii) Also in PMN, Stock *et al.* [6,7] found DS to be strong near (1, 1, 0) and accompanied by strong TA damping but also small, although still accompanied by moderate TA damping near (2, 0, 0). These authors therefore concluded that a connection exists between DS and the damping  $\Gamma_a$  of the TA phonon. However, they did not propose a conclusive physical model that would explain their observations. Recently, Phelan *et al.* [1] have shown that the unique electromechanical and dielectric features of the relaxor  $\text{Pb}(\text{Mg}_{1/3}\text{Nb}_{2/3})_{1-x}\text{Ti}_x\text{O}_3$  (PMN- $x$ PT), when compared with  $\text{Pb}(\text{Zn}_{1/3}\text{Nb}_{2/3})_{1-x}\text{Ti}_x\text{O}_3$  (PZT), could be explained by the presence of strong random electric fields (REFs) generated by the heterovalent  $\text{Mg}^{2+}/\text{Nb}^{5+}-\text{Ti}^{4+}$  cations on the B-site in PMN $_x$ PT. By contrast, the homovalent  $\text{Zr}^{4+}$  and  $\text{Ti}^{4+}$  cations on the B-site in PZT or  $\text{Ta}^{5+}$  and  $\text{Nb}^{5+}$  in KTN generate only weak or no REFs. But, unlike Pb in the lead relaxors, the K cation in KTN is not off-centered. The KTN is therefore a simpler system and offers a particularly interesting case that puts into question the explanation given above for PMN and PMN- $x$ PT. As shown below, DS is observed in KTN near the (110) BZ point but is only weak or absent near the (200) BZ point where significant TA damping is nevertheless observed [8]. In the present paper, we examine the cause of this TA damping in a neutron study of KTN.

In KTN, the  $\text{Ta}^{5+}$  ion is replaced by the isovalent  $\text{Nb}^{5+}$  ion with almost the same ionic radius, unlike PMN and PZN in which  $\text{Nb}^{5+}$  replaces the divalent  $\text{Mg}^{2+}$  and  $\text{Zn}^{2+}$  ions, respectively. Hence, chemical disordering leads to the existence of static REFs in PMN and PZN but not in KTN. Moreover, due to the heterovalency of the cations, Coulomb forces are expected to suppress long range (LR) composition fluctuations in PMN and PZN but to be absent in KTN. The KTN is therefore a useful model system for the study of relaxor ferroelectrics with homovalent cations and weak or non-existent REFs. Other such systems are  $(\text{K}_{1-x}\text{Li}_x)\text{TaO}_3$  (KLT),  $\text{Ba}(\text{Zr}_{1-x}\text{Ti}_x)\text{O}_3$  (BZT), and  $\text{Ba}(\text{Sn}_{1-x}\text{Ti}_x)\text{O}_3$  (BST), etc. The essential feature of these systems is the presence of isovalent off-center ions and the two types of dynamics in which they participate: one, the strictly local motion between crystallographically equivalent sites within the unit cell and the other the correlated/collective motion of off-center ions in different unit cells within PNRs/PNDs coupled to the soft TO mode. In KTN, the  $\text{Nb}^{5+}$  cations within each unit cell are displaced from their high symmetry site by  $0.145 \text{ \AA}$  in eight equivalent  $\langle 111 \rangle$  directions between which they can reorient [9]. These off-center ions create electric dipoles that become correlated at lower temperatures and collectively reorient under the action of an external electric field, giving rise to the characteristic relaxor behavior of the dielectric susceptibility. In addition, these are likely to give rise to localized modes (LMs) within PNRs/PNDs that can couple to the TO and TA lattice phonons.

In the present paper, we have studied the damping of the TA phonon by means of high resolution inelastic cold neutron scattering near the (200) BZ point where DS is very small [8]. We find that the TA damping is small for small wavevectors

$q$  but increases rapidly to a maximum value in the vicinity of  $q \sim 0.1$  reciprocal lattice units (r.l.u.). We show that this TA damping can be qualitatively explained by either one of two models. In the first model, it is successfully explained in terms of a resonant interaction between the TA phonon mode and a dispersionless LM of frequency  $\omega_L$  and damping  $\Gamma_L$ ,  $\Gamma_L < \omega_L$ , strongly coupled to the soft TO phonon mode (TA-[LM-TO]). The value of the frequency  $\omega_L$  is found to be close to the theoretically estimated value for the tunneling splitting of the  $\text{Nb}^{5+}$  ions in their motion between off-center positions,  $\omega_L \sim 30 \div 35 \text{ K}$  [9,10].

Alternatively, the TA damping can be successfully described in terms of an empirical Havriliak-Negami (HN) [11] relaxation, revealing a strong resonancelike transient response.

In the following, we present diffuse and inelastic neutron scattering experimental results in Sec. II, their analysis in Sec. III, and a general discussion in Sec. IV. The mathematical details of the HN model are presented in Appendix A. The interaction between tunneling off-center ions among (111) positions and the TO and TA phonons is formally described in Appendix B. Some earlier results can also be found in Refs. [12] and [13].

## II. EXPERIMENT

### A. DS in the relaxor $\text{KTa}_{0.85}\text{Nb}_{0.15}\text{O}_3$ (KTN15)

The DS measurements were made on a single crystal  $\text{KTa}_{0.85}\text{Nb}_{0.15}\text{O}_3$  (KTN15). The development of a local structural order (PNDs), with lower symmetry than the surrounding lattice, was first evidenced in the KTN15 crystal through elastic DS (within the limit of resolution). The DS measurements were carried out on the BT2 spectrometer at the neutron facility at the NCNR neutron center at the National Institute of Standards and Technology (NIST) with collimations of  $60'-40'-40'-80'$  and neutron energy of 14.7 meV. Pyrolytic graphite was used to filter out harmonics. The scattering plane was (100)-(011), and elastic scattering was measured around the (110) Bragg peak in transverse (001) scans and upon warming. The results are presented in Fig. 1(a) on two different scales, highlighting the DS on a reduced vertical scale and the full scale Bragg intensity as an inset. These elastic scattering results were fitted with two peaks: a Gaussian for the Bragg and a Lorentzian for the DS. The DS is clearly visible and seen to grow below 160 K. The Bragg peak intensity increases rapidly below 140 K due to the relief of primary and secondary extinction caused by atomic plane distortions. In Fig. 1(b), the integrated intensity of the DS is seen to reach a maximum, and its width [full width at half maximum (FWHM)] reaches a minimum at the transition,  $T_c \approx 130 \text{ K}$ . Figure 2 shows the relaxor behavior of the dielectric susceptibility. Its frequency dispersion becomes clearly visible below approximately 140 K but is weaker than in other relaxors, such as KLT. It is worth noting, however, that this frequency dispersion in KTN crystals with lower concentrations of niobium (e.g., 3%) is greater and very similar to that in PMN and PZN.

The minimum of the FWHM of the DS provides an estimate of the maximum correlation length at the transition,  $\xi(T = 130 \text{ K}) \approx 10$  unit cells  $\approx 39.5 \text{ \AA}$ . Whether the DS observed in KTN15 unequivocally indicates dynamic PNRs,

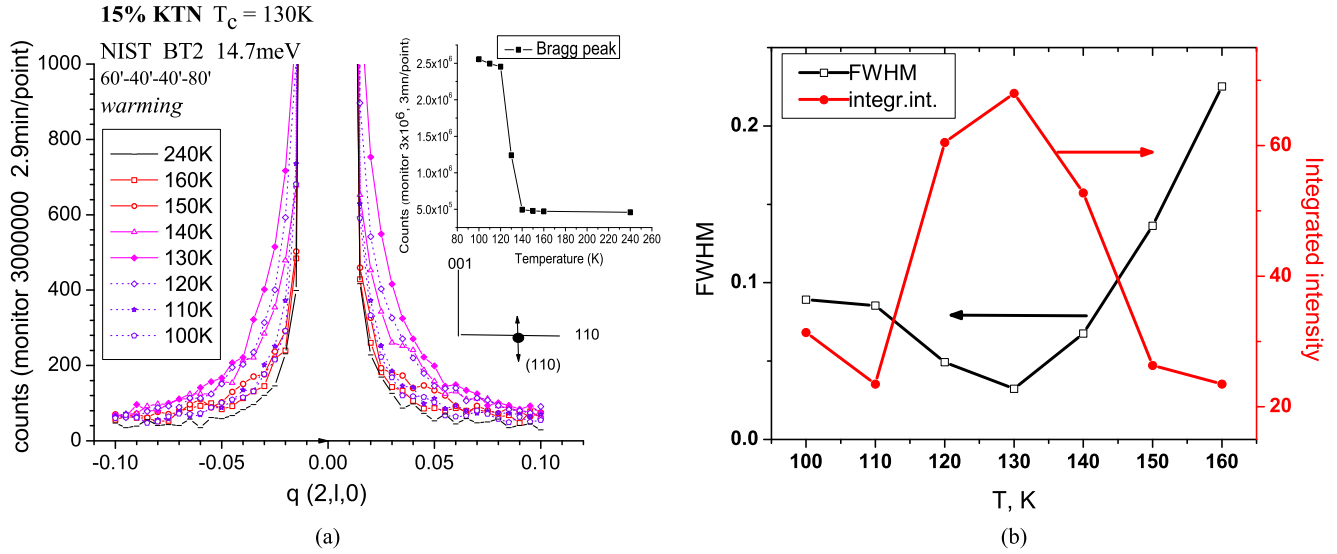


FIG. 1. (a) (110) Elastic diffuse scattering for different temperatures; inset: Bragg peak intensity vs  $T$ . (b) The FWHM and integral intensity of the DS around (110) vs  $T$ .

the formation of static PNDs (within the energy resolution of the measurement) or both PNRs and PNDs is not a completely settled question. A likely answer to this question can, however, be obtained from the results of dielectric resonance studies by one of us [14]. These resonances, which appear well above the transition, are due to polarization-acoustic strain (or piezoelectric) coupling in the paraelectric phase of KTN and other relaxors. Such a coupling should be absent in the perfect cubic phase of KTN, and its existence reveals the presence of PNDs—or static correlations of Nb ion displacements in neighboring crystal cells—and the accompanying polarization and local strain fields. In a KTN15.7%Nb crystal, for example, these resonances have been observed at temperatures as high as 200 K upon cooling under an external dc electric field and up to approximately 180 K upon zero-field heating, with a large change in amplitude around  $T^* \approx T_c + 25$  K with  $T_c \approx 139$  K [14]. Their metastability indicates that the PNDs probably form as a diffuse first order transition, similar to the condensation of water droplets in a supersaturated vapor. We should also note that, by analogy with a vapor, the presence of

static PNDs does not preclude the simultaneous presence of PNRs with dynamically correlated Nb ions.

**B. High resolution inelastic neutron scattering in KTN15**

High resolution measurements of the TA phonon in a single crystal KTN15% were also made on the SP4F2 cold neutron triple axis spectrometer at the Laboratoire Leon Brillouin in Saclay (France), near the (200) BZ point in the (100)-(010) scattering plane, with the phonon propagating in the (010) direction. Elastic neutron DS was absent at that point [13], within the limit of our resolution, but was, however, present near the (110) BZ point, as reported above. For the inelastic neutron scattering measurements, the effective collimations used were as follows: horizontally, 273'-27'-40'-40'; vertically, 51'-69'-137'-275'; and the final neutron wave vector was  $1.64 \text{ \AA}^{-1}$  from  $q = 0.025$  to  $q = 0.9$ , providing a high energy resolution of  $\sim 0.2$  meV (0.05 THz), and  $2.662 \text{ \AA}^{-1}$  at  $q = 0.12$  and  $0.16$ , providing a resolution of 1 meV. Pyrolytic graphite was also used to filter the harmonics. Several representative spectra are shown in Fig. 3 for the TA phonon with  $q = 0.025$  and  $q = 0.12$  near the (200) Bragg reflection at different temperatures in the region where DS is very small. Fitted curves are also shown, using a damped harmonic oscillator description for the phonon, including the thermal population and taking into account the combined influence of the spectrometer resolution and of the strong anisotropy of the phonon dispersion surface away from the  $\langle 100 \rangle$  direction, as indicated in the legend.

*1. The TA phonon dispersion in KTN15*

The TA phonon dispersion is presented as a function of wave vector in Fig. 4 and temperature in Fig. 5. As previously observed, the dispersion curve in Fig. 4 exhibits a kink at a frequency of  $\Omega \approx 0.7$  THz around  $q = 0.12$ , still quite far from the zone boundary, which is reproduced here by a sine function. In Fig. 5, the phonon frequency is relatively

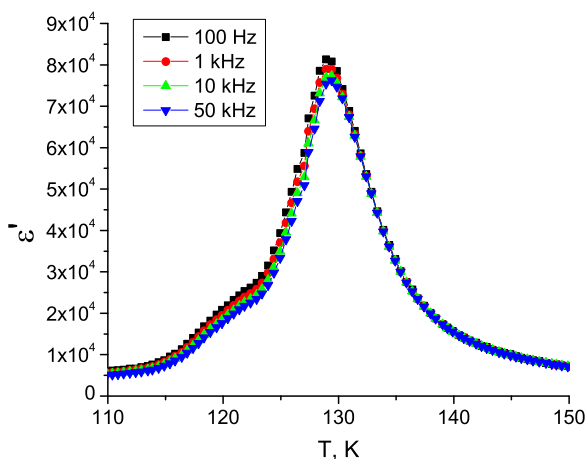


FIG. 2. Dielectric susceptibility of KTN15 vs temperature.

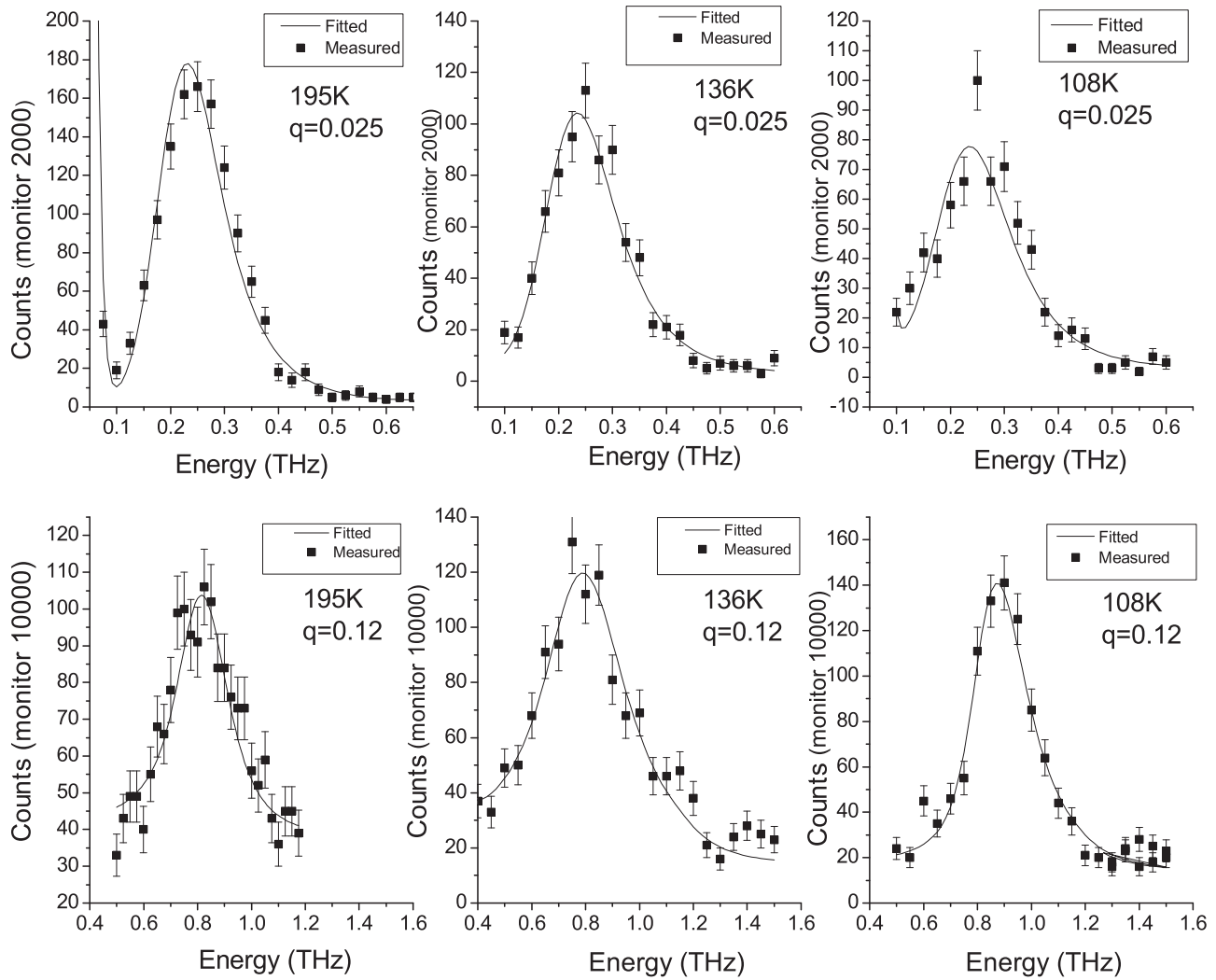


FIG. 3. Transverse acoustic phonon spectra (experimental data and fitting curves for a damped harmonic oscillator). The functional form used to fit the spectra corresponding to  $q = 0.025$  was  $\omega^2 = 26q_y^2 + 60q_x^2 + 30q_z^2$  and that for  $q = 0.12$ ,  $\omega = 0.5 + 1.5q_y + 20q_x^2 + 20q_z^2$ . The same functional form was used for all temperatures.

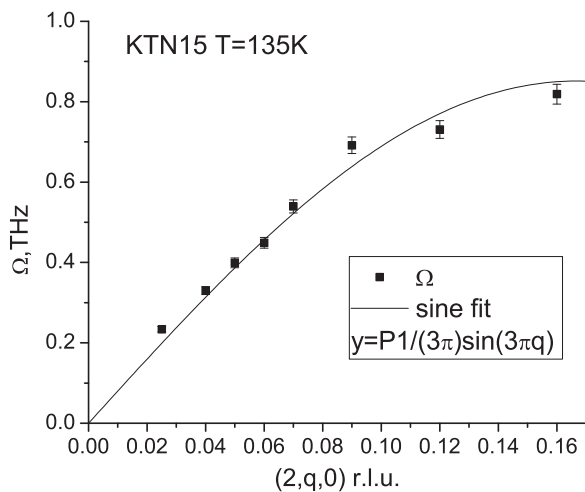


FIG. 4. The transverse acoustic wave (TAW) dispersion curve for KTN15 at  $T = 135$  K. Fitting curve  $\Omega = P1/(3\pi)\sin(3\pi q)$  with  $P1 = 8.024 \pm 0.17$  THz/r.l.u. Note the strong deviation ( $\sim 14\%$ ) from a linear dispersion, even at  $q \sim 0.1$ .

flat with temperature for small wave vectors,  $q \leq 0.07$ . But the frequency shows a clear dip around 136 K (temperature measured) for  $q \geq 0.09$  and a broad minimum also around the same temperature with a clear hardening at lower temperatures for  $q = 0.16$ . As a rule, acoustic phonon frequencies increase at low temperatures due to anharmonic interactions. Here instead, a frequency minimum is observed (especially for  $q = 0.16$ ) in the region where strong polarization fluctuations are present (PNDs).

## 2. The TAW damping in KTN15

The evolution of the TAW damping as a function of temperature is shown in Figs. 6(a) and 6(b). In Fig. 6(a), the phonon width,  $\Gamma$ , is relatively flat and independent of temperature for small wave vectors. For larger wave vectors, however,  $\Gamma$  increases with decreasing temperature and reaches a maximum for  $q \geq 0.07$  around 136 K, a temperature at which the PNDs are clearly present (see DS in Fig. 1).  $\Gamma$  then decreases significantly at lower temperatures. This temperature profile of the TA damping indicates that the lattice



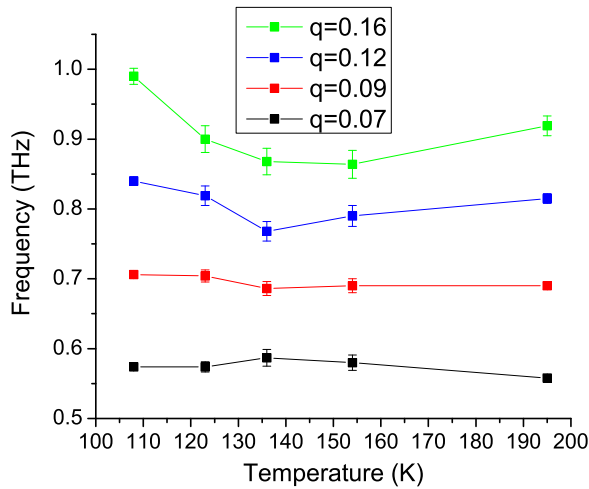


FIG. 5. The TAW ( $2, q, 0$ ): frequency vs temperature for KTN15 ( $1 \text{ THz} = 4.139 \text{ meV}$ ).

is relatively ordered at high temperature; becomes partially disordered at intermediate temperature, when the PNRs and then the PNDs are present and then scatter the TA phonons; and returns progressively to a more homogeneous although still distorted state (large Bragg intensity) below  $T_c$  as the PNDs grow and merge. It is also interesting to note that the curves corresponding to  $q \leq 0.08$  all tend to converge toward  $\approx 220 \text{ K}$ , the upper temperature limit at which the PNDs are known to appear (see dielectric resonances mentioned earlier [14] and again below).

In Fig. 6(b), the  $q$  dependence of the damping also reveals an interesting trend. At all temperatures, the phonon width exhibits a step increase around  $q = 0.07$ , goes through a shallow maximum at  $q = 0.09$ – $0.12$ , and remains high beyond. The step increase is moderate at  $195 \text{ K}$ , the highest temperature measured; maximum at intermediate temperatures around  $140 \text{ K}$ ; and significantly smaller at the lowest temperature

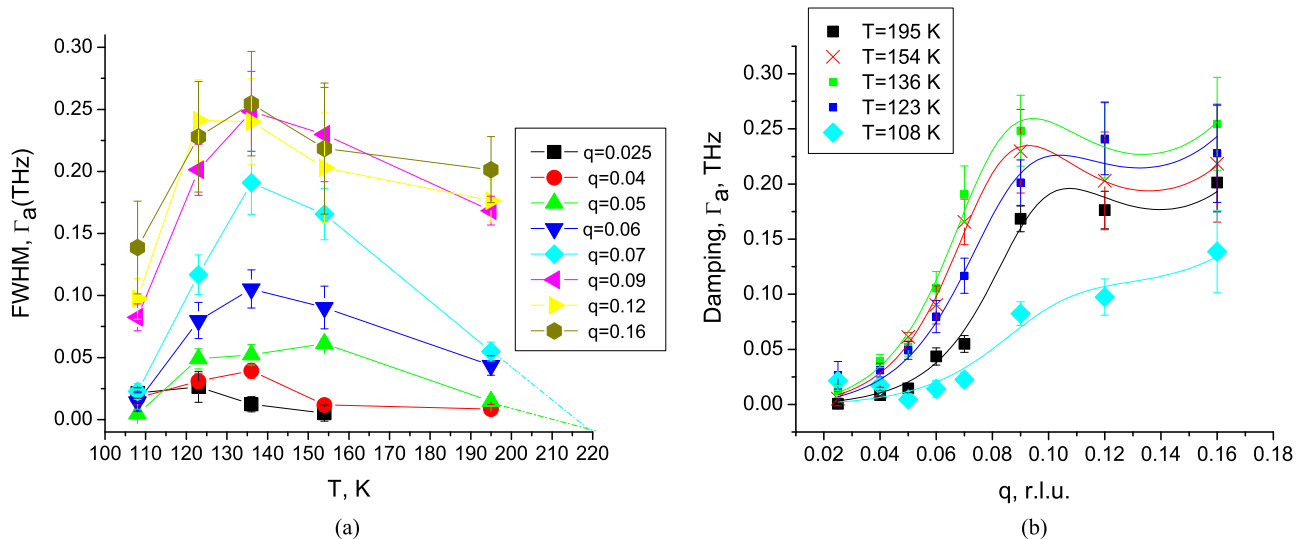


FIG. 6. (a) Damping (FWHM),  $\Gamma_a$ , of the transverse acoustic (TA) mode vs temperature for different values ( $2, q, 0$ ) in the single crystal KTN15 ( $1 \text{ THz} = 4.139 \text{ meV}$ ,  $1 \text{ meV} = 11.59 \text{ K}$ ). (b) The TA phonon damping  $\Gamma_a$  vs wave vector  $q$  at the different temperatures. Experimental data and three-parameter fit with Eq. (4) in the text. (see Sec. III A).

measured of  $108 \text{ K}$ . Such a step increase with maximum around  $q = 0.09$ – $0.12$  suggests scattering of the TA phonon by inhomogeneities of approximate size  $8 \div 11$  unit cells. As mentioned at the beginning of the paper, dynamic PNRs appear at Burns temperature,  $T_d$ , then become quasistatic or static PNDs at  $T^*$ , giving rise to DS and the characteristic frequency dispersion of the dielectric constant of relaxors. As seen in Fig. 2,  $T^* \geq 160 \text{ K}$  in KTN15. In fact, based on the observation of the dielectric resonances mentioned earlier, we conclude that PNDs probably become stable at temperatures as high as  $T = 200 \text{ K}$  in KTN15.7% upon cooling in an external electric field [14]. It is important to note that the temperature at which the PNDs are observed to appear also depends upon the characteristic frequency of the measurement, that temperature being higher for higher frequencies.

### C. Inelastic neutron scattering in KTN17

To help with the interpretation of the high resolution inelastic neutron scattering data presented here for KTN15%, additional data on the TA and soft TO phonon mode dynamics were obtained on another single crystal with a similar concentration, KTN17 (17%Nb), which exhibited similar features to those in KTN15. Measurements of KTN17 were made on the thermal neutron triple axis spectrometer BT9 at the NCNR neutron center (NIST) with fixed incident energy of  $14.7 \text{ meV}$  [15]. Constant  $q$  and constant  $E$  scans of the TO and TA phonon branches were performed along the line  $(q, 2, 0)$  in the temperature range between  $100 \text{ K}$  and  $310 \text{ K}$ . The dispersion curves obtained directly from the observed frequencies in the inelastic spectra measured at constant  $q$  and at higher temperatures ( $310 \text{ K}$  and  $240 \text{ K}$ ) are shown in Fig. 7(a). The soft TO phonon peaks are seen to be already unusually broad at these higher temperatures, as indicated by the large vertical bars. The temperature dependence of the TO phonon frequency at the  $(0, 2, 0)$  BZ point is shown in Fig. 7(b). The measured spectra are analyzed below in terms of the dynamic structural factor,  $|F(Q)|$ , which is proportional to the scattering cross

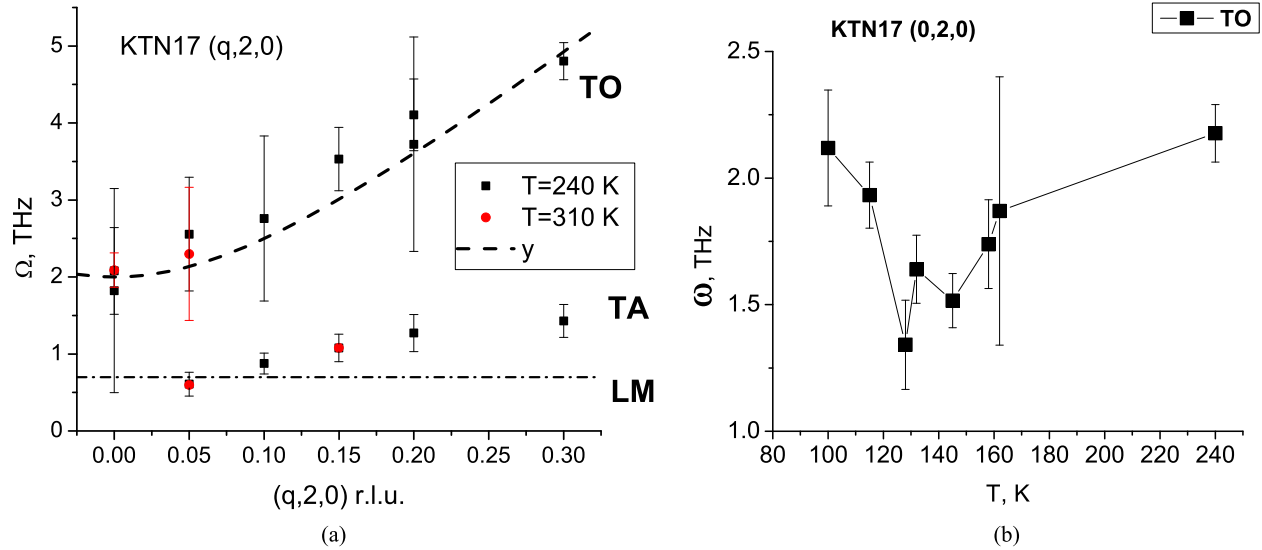


FIG. 7. (a) The KTN17: dispersion of the transverse optic wave (TOW) and TAW at  $T = 310$  K and  $240$  K. Note the large width of the TO peak (vertical bars).  $y = \sqrt{\omega_0^2 + C_o^2 q^2}$ ,  $\omega_0 = 2$  THz,  $C_o = 15$  THz/r.l.u. The dash-dot line at  $E = 2.9$  meV ( $0.72$  THz) marks the estimated energy of the dispersionless localized modes mentioned in the text. (b) The KTN17: temperature dependence of the TO phonon frequency at the  $(0, 2, 0)$  BZ point. The TO phonon is softening, but its frequency remains high even at zone center with a gap  $b \sim 1.2$  THz. The vertical bars indicate the phonon peak width.

section and is obtained from the experimental intensities,  $I$ , after correction for the Bose temperature factor and assuming an inverse square root energy dependence of the harmonic phonon displacement amplitude (see Shirane *et al.* [15]):

$$I = A \frac{1}{E(q)} |F(Q)|^2 \begin{cases} n+1 \\ n \end{cases} \text{ with } n = \frac{1}{\exp[E(q)/T] - 1}, \quad (1)$$

in which  $E$  is the phonon energy and  $A$  is a numerical factor determined by the parameters of the spectrometer. We note that the transformation given in Eq. (1) corrects for the varying scattering weight at different energies but, unfortunately, also enhances background fluctuations. We also note that effects of the spectrometer resolution are not taken into account in such a simple approach. In the following, we omit the factor  $A$  for the purpose of a semi-quantitative analysis.

Constant energy spectra measured at  $E = 4$  meV and  $6$  meV are reproduced in Figs. 8 and 9. These two energies were conveniently chosen to separately probe the behaviors of the TAW ( $4$  meV) and TOW ( $6$  meV). As seen in Fig. 8(a) for  $E = 4$  meV, the overall TA phonon intensity is smaller in the temperature range  $130$  K  $< T < 160$  K, with significant intensity present at the zone center,  $q = 0$ . The  $F^2$  returns to a more usual phonon spectral shape at  $100$  K. The same TA phonon curves are presented in a more detailed manner and fitted with damped harmonic oscillator functions in Figs. 8(b) and 8(c) at  $T = 130$  K and  $100$  K, respectively. Note that the different peak shapes for positive and negative  $q$  are only an effect of the spectrometer resolution (focusing for positive  $q$  and defocusing for negative  $q$ ).

Constant  $E$  spectra taken at  $E = 6$  meV and fitted peaks are shown in Fig. 9. At this energy, only one peak corresponding to the TO phonon is observed in the spectra, consistent with

the dispersion curves shown in Figs. 7(a) and 7(b). (Note: The two peaks at  $T = 130$  K correspond to the same phonon at positive and negative  $q$ .) The width of the TO phonon peak is seen to increase or, equivalently, the correlation length of the TO phonon is seen to decrease with temperature. The high background at  $130$  K and  $100$  K points to a very broad distribution of intensity in  $q$  space, corresponding to a very short correlation length, or localized excitations (LM). In Fig. 9(c) at  $100$  K, the TO peak is absent.

In trying to understand the origin of the TA phonon damping in KTN15, the main experimental results obtained on the KTN15 and KTN17 single crystals are as follows:

- (1) a deviation from the linear dependence in the TA dispersion curve,  $\omega$  vs  $q$ , between  $q \approx 0.1$  and  $0.16$  and a broad minimum in the TA frequency around the transition temperature,  $T = 135$  K, in this same  $q$  range;
- (2) a steplike increase in TAW damping with inflection point around  $q = 0.07$ ;
- (3) maximum TA damping at  $T = 135$  K for  $q$  between  $0.12$  and  $0.16$ ;
- (4) a high minimum of the TO mode frequency near the transition; and
- (5) no observed crossing of the TA and soft TO phonon branches, at least for  $q \leq 0.16$ , but crossing of the TA phonon branch and a dispersionless branch of localized excitations (LM).

In the following analysis, we show that the high frequency of the soft TO mode in the transition region,  $T < 160$  K, is due to its strong coupling to localized excitations (LM) whose flat branch at  $\omega_L = 0.7$  THz crosses the TA curve. These localized excitations can be attributed to the collective reorientational motion of the off-center Nb ions within each PNR/PND through tunneling. The TA damping is then due to scattering of the TAW by mixed TO-LM excitations.

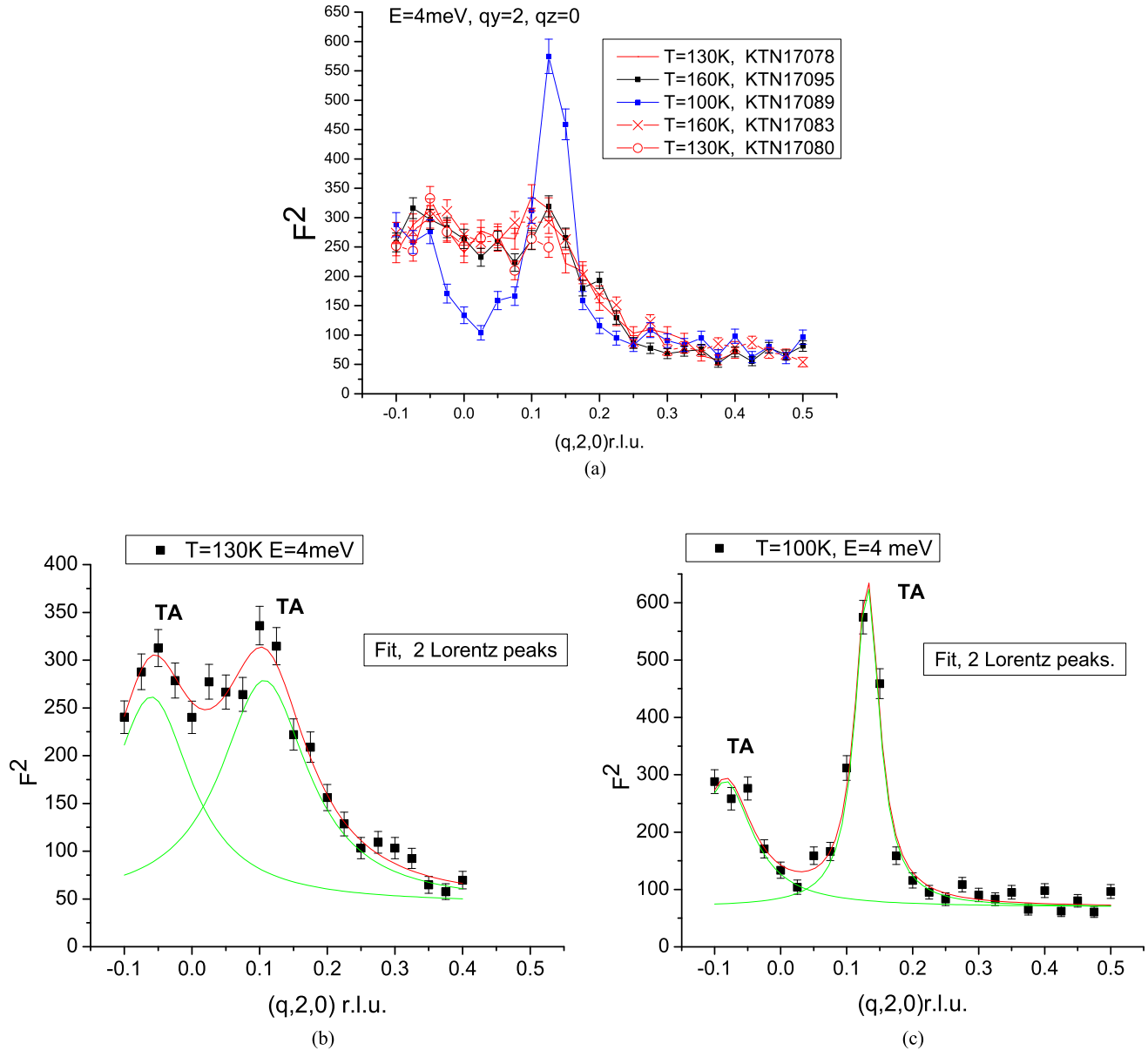


FIG. 8. (a) The KTN17:  $q$  scan at constant energy, for several temperatures upon cooling and warming ( $E = 4$  meV = 0.966 THz). (b) The KTN17:  $T = 130$  K. The  $q$  scan at constant energy,  $E = 4$  meV. Fit: two Lorentz peaks, positions  $q_{c1} = 0.107$ ,  $q_{c2} = -0.06$ ; widths  $w_1 = 0.158$ ,  $w_2 = 0.144$ ; areas  $A_1 = 58$ ,  $A_2 = 49$ . (c) The KTN17:  $T = 100$  K. The  $q$  scan at constant energy,  $E = 4$  meV. Fit: two Lorentz peaks, position  $q_{c1} = -0.084$ ,  $q_{c2} = 0.131$ ; width  $w_1 = 0.1$ ,  $w_2 = 0.045$ ; area  $A_1 = 34.5$ ,  $A_2 = 39.5$ .

### III. ANALYSIS OF RESULTS

#### A. Theoretical analysis of the TAW resonant damping

The central experimental facts that we seek to explain are as follows: the TA phonon broadening with decreasing temperature; its maximum damping in the temperature range in which PNDs are present; and its return to low damping at low temperatures, despite little or no DS near the (200) reflection in KTN [8]. The model presented below and in the appendices that explains these experimental results is inspired by the model proposed by Axe *et al.* [16], who considered the effect of a direct bilinear TA-TO interaction on the TA dispersion in the incipient ferroelectric  $\text{KTaO}_3$ . In the paraelectric phase, the Hamiltonian term describing the TA-TO interaction was taken

to be proportional to the product of the two momenta (TA and TO). In the ferroelectric phase, this term was written as the product of the polarization  $P$  and a TA momentum, a product that is particularly large for long-wavelength excitations. Here, we follow a similar approach but additionally take into account the mixing of the TO and LM modes as well as the local polarization  $P$  that develops with PNRs/PNDs. We thus write an interaction Hamiltonian,  $H_{fr}$ ,

$$\begin{aligned}
 H_{fr} &= 2f(P\xi)_{ik}u_{ik} \quad \text{with} \\
 (P\xi)_{ik} &\equiv 1/2(P_i\xi_k + P_k\xi_i - 2/3\delta_{ik}(P\xi)), \quad \text{and} \\
 u_{ik} &\equiv 1/2(\partial u_i/\partial r_k + \partial u_k/\partial r_i - 2/3\delta_{ik}\text{div}(u)), \quad (2)
 \end{aligned}$$

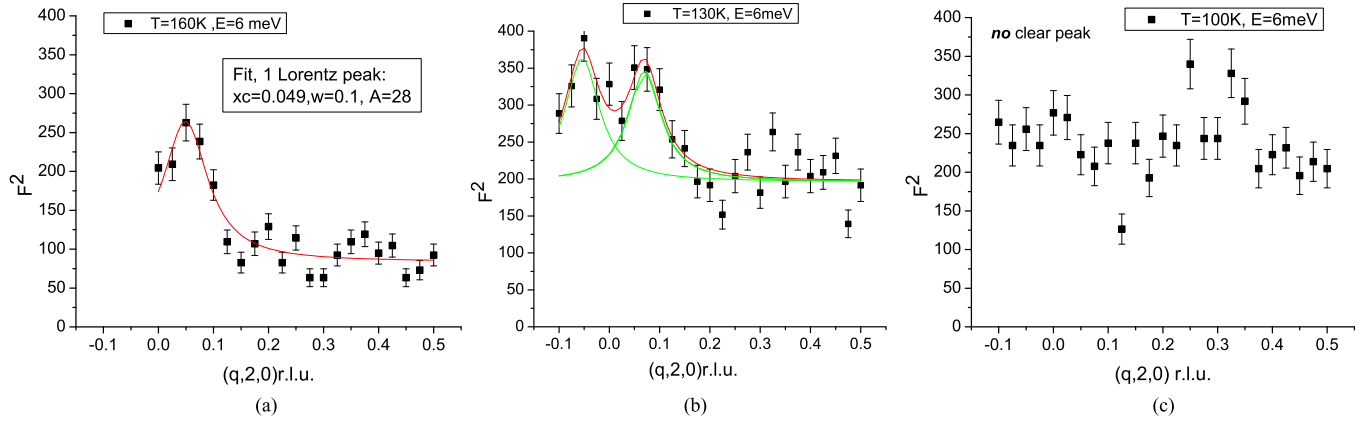


FIG. 9. The KTN17: the  $q$  scan of the TO phonon at constant energy,  $E = 6$  meV at (a)  $T = 160$  K, the correlation length is  $L = 1/w = 101$  l.u.  $\approx 40$  Å; (b)  $T = 130$  K, two Lorentz peaks are seen on higher background; (c)  $T = 100$  K, no peak but only a high background.

in which  $\xi_k$  and  $u_k$  are the  $k$  components of the TO and TA (shear) mode displacements, respectively, the parameter  $f$  is the coupling constant, and  $(P\xi)_{ik}$  and  $u_{ik}$  are written as traceless tensors with  $\delta_{ik}$  the Kronecker delta. As shown in Appendix B (B8), the LM modes that are associated with transitions between  $\text{Nb}^{5+}$  tunneling states can only become excited by the TA phonon with the appearance of the quasistatic or static polarization  $P$  of PNRs/PNDs. The existence of such a condition was revealed early in the ultrasonic results obtained by Knauss *et al.*, which showed that the coupling between a transverse ultrasonic wave and the tunneling Nb ions was only initiated by the appearance of the PNDs [16]. The similarity of our Eq. (2) with that used in Axe *et al.* [16] is not a direct one but only a formal one because  $\xi_k$  here represents a component of the renormalized TO mode eigenvector, taking into account the strong TO-LM interaction mentioned earlier. In the following, TO and LM refer to the renormalized modes resulting from this interaction. The normally soft TO mode is renormalized toward higher frequencies and the LM modes in our case toward lower frequencies (level repulsion) where they interact with the TA phonon, causing its observed damping. We work here in the approximation of a homogeneous medium and neglect in first order approximation any dispersion of the resonance. Also, unlike the TO-LM interaction, we suppose that the interaction between the TAW and the mixed LM modes is not strong (weak coupling approximation). Assuming the simplest form of a plane TA wave propagating along the  $z$  axis, polarized along the  $x$  axis, and interacting with the mixed LM mode polarized along the same  $x$  axis, the Lagrangian  $\Lambda$  and dissipative function  $\Psi$  can be written as

$$\begin{aligned} \Lambda &= \int L d^3r, L \equiv 1/2(\partial u/\partial t)^2 - C_a^2/2(\partial u/\partial z)^2 \\ &\quad + 1/2(\partial \xi/\partial t)^2 - (\omega_L^2/2)\xi^2 - fP_z\xi(\partial u/\partial z), \\ \Psi &= 1/2 \int \Gamma_L(\partial \xi/\partial t)^2 d^3r, \end{aligned} \quad (3a)$$

in which  $C_a$  is the acoustic velocity of sound. The coupled equations of motion for the TA and LM mode with momentum  $q$  and frequency  $\omega$  can then be obtained from the Lagrangian

equations, respectively, for  $u$  and  $\xi$  as

$$\begin{aligned} (\omega^2 - \omega_a(q)^2)u + ifqP_z\xi &= 0, \quad \text{with } \omega_a(q) = C_aq \\ -ifqP_zu + (\omega^2 - \omega_L^2 + i\omega\Gamma_L)\xi &= 0, \end{aligned} \quad (3b)$$

in which  $\omega_a(q)$  and  $\omega_L$  are the frequencies of the TA and LM, respectively,  $\Gamma_L$  is the damping of the LM,  $P$  the quasistatic or static polarization from PNRs/PNDs, and  $f$  is the coupling constant. It is clear from these equations that  $u$  and  $\xi$  are coupled only in the presence of  $P$ . Solving these coupled equations using perturbation theory to the first nonvanishing order in  $f$ , we obtain the following expression for the acoustic damping:

$$\begin{aligned} \Gamma_a(q) &\approx M^2q^2 \frac{\Gamma_L}{(\omega_a(q)^2 - \omega_L^2)^2 + \omega_a(q)^2\Gamma_L^2} \quad \text{with} \\ M^2 &= f^2P_z^2/2. \end{aligned} \quad (4)$$

It is interesting to note that this damping is proportional to the square of the oscillator strength,  $M$ , itself proportional to the local polarization,  $P$ , from PNRs/PNDs. The experimental TA damping data shown in Fig. 6(b) are fitted with expression (4), taking into account the sine approximation shown in Fig. 4 for the TA mode dispersion  $\omega(q)$  and considering  $\omega_L$ ,  $\Gamma_L$ , and  $M$  as fitting parameters. The values of the fitted parameters are presented in Figs. 10(a) and 10(b). The temperature dependencies of the frequency and width of the resonance are seen to be moderate. By contrast, its oscillator strength,  $M$ , exhibits a strong temperature dependence [ $M^2(T = 136 \text{ K})/M^2(T = 108 \text{ K}) \sim 2.7$ ], which mirrors the experimentally determined TA damping shown at Fig. 10(b). The maximum of the TA phonon damping can thus be attributed to the resonance maximum of the TA-LM coupling, which is discussed below.

## B. The TAW damping as due to coupling to a relaxation

Alternatively, the temperature and wave vector dependence of the TA damping can be described phenomenologically as due to the direct coupling between the TAW and a purely relaxational LM, distinct from the resonance mode described in expression (4). In the framework of the standard Debye relaxation model, the TAW damping would be written as



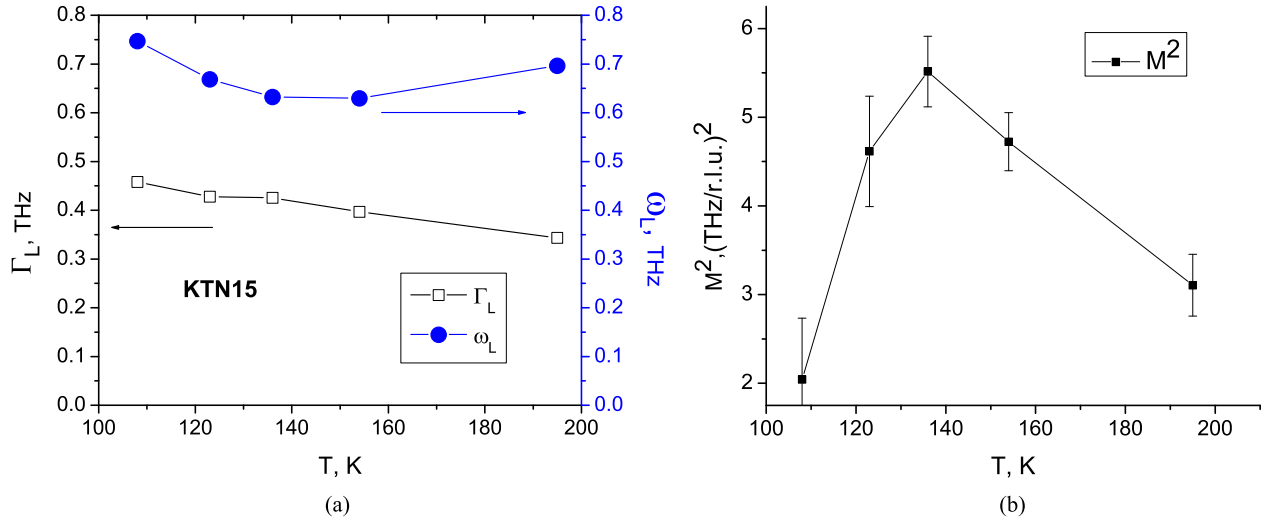


FIG. 10. (a) Frequency and width of the localized mode vs temperature, obtained by fitting the experimental data in Fig. 6(b); note that  $\Gamma_L < \omega_L$  at all temperatures. (b) Oscillator strength  $M^2$  vs temperature.

follows:

$$\Gamma_a(q) = qG_D \frac{\omega(q)\tau_D}{1 + [\omega(q)\tau_D]^2}. \quad (5)$$

Here,  $\omega$  is the frequency of the TAW,  $\tau_D$  designates the relaxation time of the LM, and  $G_D$  is a numerical factor. With the dispersion  $\omega(q)$  of the TAW taken from the experimental data shown in Figs. 4 and 5, the TA damping curves can be fitted with only two free parameters,  $\tau_D$  and  $G_D$ . However, such a simple Debye-type relaxation is found to be unable to reproduce the steplike increase observed in the measured TAW damping around  $q = 0.07$ . Instead, the presence of PNRs/PNDs suggests a distribution of relaxation times. Assuming such a distribution, the TA phonon damping can be described in the framework of the HN relaxation model for the permittivity,  $\chi(\omega)$  (see Refs. [11], [17], and [18]), which is an empirical modification of the Debye model with two exponents  $\alpha$  and  $\beta$ . The exponent  $\alpha$  is a measure of the distribution of relaxation times, and  $\beta$  introduces an asymmetry in the distribution ( $\beta = 1$  for a symmetric distribution):

$$\chi(\omega) = \chi_\infty + \frac{\Delta\chi}{[1 + (i\omega\tau)^\alpha]^\beta} \quad \text{with} \quad \Delta\chi = \chi_s - \chi_\infty, \quad (6)$$

in which  $\chi_\infty$  is the high frequency limit of the permittivity,  $\chi_s$  is the static low frequency permittivity, and  $\tau$  is a characteristic average relaxation time. Special cases of the HN relaxation function correspond to the Debye ( $\alpha = \beta = 1$ ), Cole-Cole ( $0 < \alpha < 1$ ,  $\beta = 1$ ), and Cole-Davidson ( $\alpha = 1$ ,  $\beta \neq 1$ ) processes. The Cole-Cole relaxation is often used to describe the so-called stretched relaxation observed in glasses and polymers.

As shown in Figs. 11(a) and 11(b), using, as before, the sine approximation to the TA phonon dispersion,  $\omega(q)$ , shown in Fig. 4, the TA phonon damping can be fitted with excellent accuracy by the imaginary part of the susceptibility expression (6), with  $\beta = 1$  and three free parameters,  $P$ ,  $\tau$ , and  $\alpha$  with

$\alpha \approx 3/2$ :

$$\Gamma_a(q) = qP \frac{[\omega(q)\tau]^\alpha \sin(\pi\alpha/2)}{1 + 2[\omega(q)\tau]^\alpha \cos(\pi\alpha/2) + [\omega(q)\tau]^{2\alpha}}. \quad (7)$$

The fitting parameters are plotted in Figs. 11(c) and 11(d). Both  $P$  and  $\tau$  are seen to reach a maximum in the region of the transition and to drop rapidly below, while  $\alpha$  decreases to reach a constant value below the transition. Both tendencies suggest a freezing of the relaxation, with the faster components of the distribution remaining dynamic to a lower temperature.

We now discuss specific features of the HN function connected with the value of the exponent  $\alpha$ . Comparing the Debye,  $f_D$ , and HN,  $f_{\text{HN}}(\beta = 1)$  relaxation functions,

$$f_D = 1/(1 + i\omega\tau) \quad \text{and} \quad f_{\text{HN}} = 1/(1 + (i\omega\tau)^\alpha), \quad (8)$$

$f_{\text{HN}}$  with  $\alpha = 1/2$  (i.e.,  $< 1$ ) can be shown to slowly decreases for  $\omega\tau \gg 1$ , which is often described as a stretched relaxation in the literature of glasses and polymers. The same function  $f_{\text{HN}}$  exists but with  $\alpha \approx 3/2$  (i.e.,  $> 1$ ), as in the present case, gives rise to a resonancelike transient oscillation, which is responsible for the steplike increase in the TAW damping observed experimentally around  $q = 0.07$ .

In the time domain, the Debye relaxation function monotonically drops to zero with time:

$$F_D(t) \equiv \frac{1}{2\pi} \int_{-\infty}^{\infty} \frac{\exp(i\omega t)}{1 + i\omega\tau} d\omega,$$

$$F_D(t < 0) = 0 \quad \text{and} \quad F_D(t > 0) = \frac{1}{\tau} \exp(-t/\tau). \quad (9)$$

By contrast, the HN relaxation function with  $\alpha > 1$  exhibits a resonancelike transient oscillation at short times. Its time-domain representation,  $F_{\text{HN}}(t)$ , is shown in Fig. 12 and can be expressed by means of the Mittag-Leffler function  $E_\alpha(x)$  for the case  $\beta = 1$  [17,18].

The resonancelike transient relaxation indicates that the HN function  $f_{\text{HN}}(\alpha = 3/2, \beta = 1)$  (8) has a pole in the complex  $\omega$ -plane (see Appendix A for details) and can also be adequately fitted at short times by a Lorentzian function, as

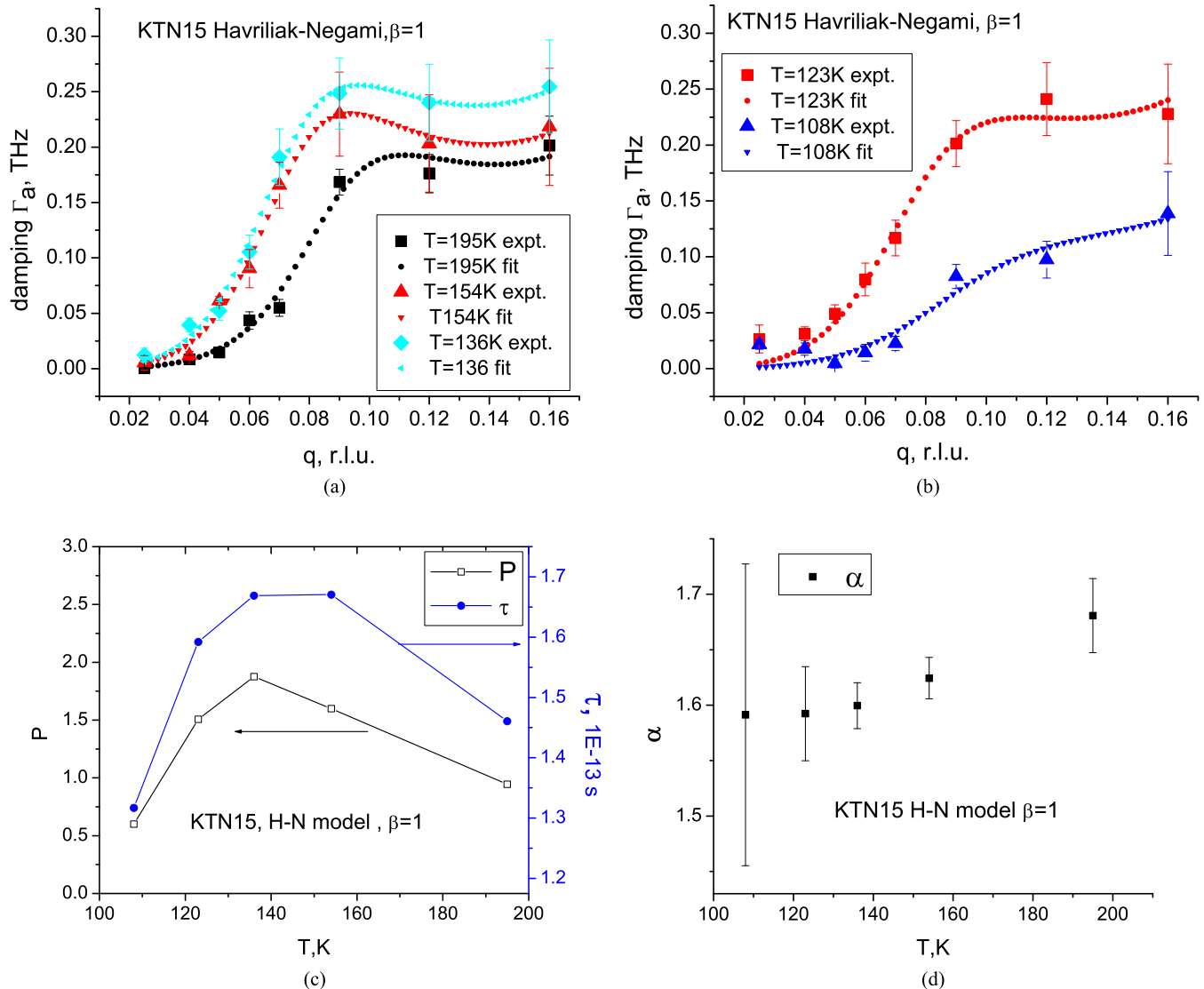


FIG. 11. (a) Experimental data and fit with expression (6) for the Havriliak-Negami relaxation model with  $\beta = 1$  at  $T = 195$  K, 154 K, and 136 K. (b) Same as in Fig. 12(a) but at  $T = 123$  K and 108 K. A steplike increase in the TAW damping around  $q = 0.07$  is precisely reproduced in this H-N model. (c) Values of the fitting parameters  $P$  and  $\tau$  vs temperature using the Havriliak-Negami relaxation model in Eq. (7) with  $\beta = 1$ . (d) Value of the fitting exponent  $\alpha$  vs temperature using the Havriliak-Negami relaxation model in Eq. (7) with  $\beta = 1$ .

illustrated in Fig. 12. Another significant difference between the  $f_D$  and  $f_{HN}$  relaxation functions is worth mentioning. A Debye relaxation is a localized process in which each unit relaxes independently of the others after several rapid initial collisions. In the high-frequency range,  $\omega\tau \gg 1$ , or at short times,  $f_D(\alpha = 1)$  can be expanded in terms of integral powers of the parameter  $1/(\omega\tau)$ , while  $f_{HN}(\alpha = 1/2)$  is expanded in terms of half powers,  $1/(\omega\tau)^{1/2}$ . This point was carefully investigated in the context of high-viscosity liquids. A detailed theory was proposed by Isakovitch and Chaban [19] who regarded these liquids as microinhomogeneous media whose dynamics are controlled by diffusion, as in a delocalized or nonlocal process. Letting  $R$  designate the characteristic size of a microformation or a diffusion length in the viscous liquid, the long wave response of such a medium to an excitation with wave vector  $q$  will be determined by the value of the dimensionless parameter  $(qR)$ , or equivalently by the value

of  $(\omega\tau)^{1/2}$ . As discussed in the second part of the Discussion section below,  $\alpha \approx 3/2$  indicates that the local relaxation of the polarization has now become slower than its diffusion time, and the relaxation is therefore delocalized or a collective process.

#### IV. DISCUSSION

We have studied the damping  $\Gamma_a$  of the TA phonon in the relaxor KTN with moderate niobium concentrations of 15%–17% by means of high resolution inelastic cold neutron scattering. The TA phonon linewidth or damping exhibits a step increase around momentum  $q = 0.07$ , goes through a shallow maximum at  $q = 0.09$ – $0.12$ , and remains high beyond and up to the highest momentum studied of  $q = 0.16$ . This step increase is moderate at 195 K, the highest temperature measured; maximum at intermediate temperatures around

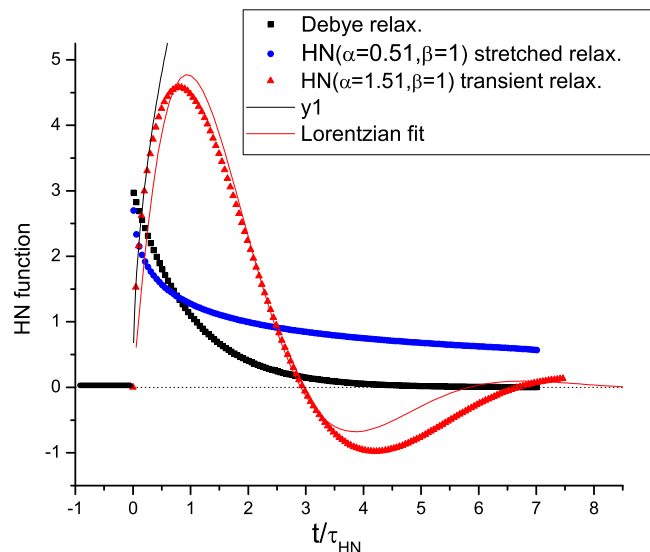


FIG. 12. Time evolution of the Debye, stretched HN (with  $\alpha = 0.51$ ,  $\beta = 1$ ) and transient HN relaxation (with  $\alpha = 1.51$ ,  $\beta = 1$ ), and Lorentzian fit  $y = A \times \exp(-t/\tau_{\text{HN}}/t_1) \sin(\pi t/\tau_{\text{HN}}/t_2)$  with  $A = 10.56$ , and the dimensionless scaling factors  $t_1 = 1.49$  and  $t_2 = 2.92$ . The value of the ratio of the damping and oscillation arguments of the Lorentzian function  $(t/\tau_{\text{HN}}/t_1)/(\pi t/\tau_{\text{HN}}/t_2) \div 0.624$  is close to the value  $1/\sqrt{3} = 0.5773$  of the pole term (A3) in Appendix A. For  $t/\tau_{\text{HN}} < 0.35$ , the HN function can be approximated as  $y_1 = 6.7838(t/\tau_{\text{HN}})^{1/2}$ . For convenience, the Debye and stretched relaxation curves are displaced.

140 K; and significantly smaller at the lowest temperature measured of 108 K.

The observed TAW damping is successfully fitted in the framework of the simple model, described above, of the TA phonon interacting with a mixed LM-TO mode. From fitting the data in Fig. 6(b) using Eq. (4), the bare LM is found to have frequency  $\omega_L \sim 0.6 \div 0.7$  THz and damping  $\Gamma_L \leq \omega_L$  [Fig. 10(a)]. Maximum scattering of the TAW occurs when the frequency of the acoustic phonon is resonant with the LM,  $\omega_a \approx \omega_L$ . The bare frequency of the LM mode,  $\omega_L$ , depends only moderately on temperature (variation  $\leq 15\%$ ), and the variation of  $\Gamma_L$  with temperature is less than 30%. However, the oscillator strength  $M$ , shown in Fig. 10(b), exhibits a strong maximum in the temperature range  $\sim 120$  K  $\div$  160 K, which is also the temperature range of the dielectric relaxation maximum (relaxor behavior).

We now address the possible nature of the resonant LM in KTN. As suggested earlier, the existence of such a mode is connected with the presence of off-center  $\text{Nb}^{5+}$  ions, displaced from their high symmetry sites by  $0.145 \text{ \AA}$  in one of eight equivalent  $\langle 111 \rangle$  directions inside PNRs/PNDs [9]. The off-center Nb ions undergo two types of dynamics, on two distinct time scales: The first one is associated with the TO mode, and the second one is associated with the tunneling motion of the  $\text{Nb}^{5+}$  off-center ions within each unit cell. Whereas the intrinsic soft TO branch would normally tend toward zero at the center of the BZ, here the observed TO phonon frequency remains high even at the zone center with a gap  $b \sim 1.2$  THz [Fig. 7(b)]. Such a gap in the soft TO mode

spectrum has also been observed in other materials [20–23]. In  $\text{SrTiO}_3$  [20], the gap  $\omega^\infty \approx 0.13$  THz ( $T_c \approx 105$  K) was attributed to the interaction between the TO phonon and an unspecified relaxation mode [central peak (CP) theory]. Halperin and Varma [21,22] explained the existence of the CP in terms of an interaction of the soft mode with a relaxing defect cell. They found that a *small* concentration of such defect cells in which the order parameter relaxes slowly between different equivalent orientations may account for the narrow CP as well as for the temperature dependence of the soft-mode frequency near structural phase transitions. Although significantly larger than in  $\text{SrTiO}_3$ , the gap  $b$  in KTN could similarly be attributed to the presence of an additional spectral density in the TO-TO phonon correlation function, and Halperin and Varma’s approach might apply qualitatively to the case of KTN crystal. However, the much larger value of the gap  $b \sim 1.2$  THz near the (020) BZ point and of the Nb concentrations in KTN crystals suggests an additional mechanism, this one between the TO phonon and the dispersionless LM excitations with energy  $\sim 0.7$  THz attributed to the collective tunneling motion of the  $\text{Nb}^{5+}$  off-center ions within PNRs/PNDs. The dynamics of the off-center Nb ions would seem to correspond to a resonance rather than to a relaxation. It is worth noting that, somewhat similar to the present case, the interaction of the TAW with local excitations (translation-rotation coupling) has been evidenced in orientationally disordered crystals and explained in terms of dipole-dipole interactions (see reviews [24,25]). In the present case of relaxor dynamics, however, long range (LR) dipole-dipole interactions should have only a moderate effect. Finally, CPs have been reported in light scattering studies of liquids where they have also been attributed to relaxation processes [31].

#### Pseudospin model of the TA-[TO-LM] interaction

The model discussed below rests on the assumption that the  $\text{Nb}^{5+}$  ions are likely involved in both the acoustic TA and the soft optic TO motion as well as in their own tunneling motion and/or thermally activated jumping between equivalent sites. Girshberg and Yacoby [10,26] have described the dynamics of such a system of off-center ions in terms of pseudospins. A similar formal approach has been applied to order-disorder ferroelectric transitions [27]. Pseudospin dynamics is usually described in the framework of the Ising model with a spin Hamiltonian that includes a transverse field,  $H_T$  [26],

$$H = -\Omega \sum_m \sigma_m^x - \frac{1}{2} \sum_{m,m'} J(m-m') \sigma_m^z \sigma_{m'}^z + H_T. \quad (10)$$

Here  $m$  is the position index,  $\sigma_m$  is the Pauli spin matrix,  $J(m-m')$  is the direct spin-spin interaction constant, and  $\Omega_0$  is the tunneling frequency of an individual off-center ion between different orientations. The term  $H_T$ —the heat reservoir—includes the interaction of the spins with all thermal excitations, namely thermal phonons, but excluding the TO phonon, which is being considered separately. The strength of the direct spin-spin interaction  $J(m-m')$  is assumed to be moderate. Nevertheless, spin-spin interactions through a virtual TO mode are essential and become particularly strong near the transition as the bare TO phonon softens toward the dispersionless LM branch. In KTN, Girshberg

and Yacoby [10,26] estimated the value of the individual  $\text{Nb}^{5+}$  ion tunneling splitting between off-center positions to be  $2\Omega \sim 30 \div 34 \text{ K} = 0.625 \div 0.709 \text{ THz}$ . This is almost exactly the value of  $\omega_L$  obtained in Fig. 6(b) from fitting the TA damping and is also shown in Fig. 10(a) as a function of temperature.

We now formally describe the nature of the interaction between the TA and the TO phonon coupled to the LM. Because of their small off-center displacement and corresponding dipole moment, the direct electric dipole-dipole interaction between  $\text{Nb}^{5+}$  off-center ions can be regarded as moderate compared with their interaction with the TO phonon and, in first order approximation, we can write the system wavefunctions in terms of individual off-center Nb ions tunneling between eight equivalent (111) positions. As indicated in Appendix B, the fully symmetric ground state wave function corresponds to a superposition of all equivalent eight positions:  $\psi_S = [1, 1, 1, 1, 1, 1, 1, 1]$ , with energy  $\langle \psi_S | H | \psi_S \rangle = -3\Omega$ . Similarly, the first excited state is a triplet,  $X\psi_S, Y\psi_S, Z\psi_S$ , with energy  $-\Omega$ ; the second excited state is also a triplet,  $XY\psi_S, YZ\psi_S, XZ\psi_S$ , at  $+\Omega$ ; and the third one is a singlet state,  $XYZ\psi_S$ , at  $+3\Omega$ . Thus, the initially degenerate ground state splits into eight eigenlevels of the Hamiltonian  $H$ . However, it is important to note that the corresponding wave functions are orthogonal and that transitions between these various energy levels will only occur in the presence of a perturbation,  $V$ , by either a TO or TA phonon or the quasistatic or static polarization  $P$  from PNRs/PNDs. The various possible terms and transitions are presented and discussed in Appendix B.

Because the  $\text{Nb}^{5+}$  ions are only off-centered from their high symmetric crystallographic position by a relatively small  $R_{\text{Nb}} = 0.145 \text{ \AA}$  in a (111) direction, we can expand the interaction of the TO and TA phonons with the tunneling  $\text{Nb}^{5+}$  ions in terms of the small dimensionless parameter  $r_{\text{Nb}} \equiv R_{\text{Nb}}/1. \text{u.} = 0.036 \ll 1$ . The first order term in the expansion,  $V^{(1)}[\text{TO}|\text{short range (SR)}] \sim r_{\text{Nb}}$ , describing the TO phonon-off-center Nb interaction (B4), excites dipolar transitions with energy  $2\Omega \approx 0.6 \div 0.7 \text{ THz}$  and leads—in combination with the anharmonic TO-TO interaction—to the opening of the gap  $b$ . The second order term,  $V^{(2)}(\text{TO}|\text{SR}) \sim r_{\text{Nb}}^2$ , excites quadrupolar transitions with energy  $4\Omega \approx 1.2 \div 1.4 \text{ THz}$ . However, the probability of this transition is small, especially near the BZ center, where the gap opens in Fig. 7(b). Because  $r_{\text{Nb}} \ll 1$ , it is therefore reasonable to expect that the first order term (dipolar transition) will dominate. But Eqs. (B8)–(B10) show that the TA phonon will excite transitions with energy  $2\Omega$  only if the system is at least partially polarized, i.e., in the presence of PNRs/PNDs. We therefore can expect that the TA phonon damping [at  $2\Omega = \omega_L \approx 0.6 \div 0.7 \text{ THz}$ ; Figs. 11(a) and 11(b)] will be small at high temperature, in the absence of PNRs/PNDs, maximum at  $T \sim 140 \text{ K}$  near the transition in the presence of PNRs/PNDs, and decreasing at low temperature. The TA phonon could also excite transitions with energy  $4\Omega$  due to the interaction  $V(\text{TA}|\text{SR}) \sim r_{\text{Nb}}^2$  of an elastic dipole (tensor) with acoustic stress (B6) and (B7). However, such high-energy TA phonons are not observed in our experiment (Fig. 8). A detailed analysis of the TO-LM interaction effect on the genesis of the PNRs/PNDs in KTN is outside the scope of the present paper and will be published subsequently.

### TAW damping and DS

We finally return to the question of the correlation between the TAW damping and DS. Stock *et al.* [6] pointed out the existence of a correlation between their DS results and the TAW damping in the relaxor PMN. These authors showed that strong DS near the (110) BZ point was accompanied by heavy damping and even overdamping of the TA phonon. Based on this result, they concluded that a firm connection occurs between DS and TA damping at a particular BZ point. Recently however, Stock *et al.* [7] have also reported in a PMN single crystal a moderately damped TA phonon ( $\Gamma/\omega \sim 0.3 \div 0.4$  at  $q = 0.21$ ) near the (200) reflection where DS is small or absent, as in our KTN results. Therefore, their results and ours may not be in contradiction with each other, and the connection between the DS and the TAW damping is not a necessary one but may depend on the particular situation.

We noted in the Introduction that Hirota *et al.* [5] explained their neutron DS data in PMN by proposing that DS was not necessarily due to a condensed soft TO mode but could also be due to a collective shift  $\delta$  of all the atoms within a PNR along the local polar direction. What can be said of DS in KTN in light of the above discussion? Is there a  $\delta$  shift in KTN as in PMN [4]?

One of us has previously shown that a LM can be described as a *coherent* superposition of the TO and TA phonons [28], which is similar to the collective shift  $\delta$  along the polarization direction proposed by Hirota *et al.* [5]. However, such a shift is only possible in the case of a strong TO-TA interaction. Although there is presently no definite information regarding the strength of the TA-TO interaction in KTN, recent observations of characteristic electromechanical resonances in several relaxor ferroelectrics by Pattnaik and Toulouse [14,29] [ $\text{K}_{1-x}\text{Li}_x\text{TaO}_3$  (KLT), KTN, and PZN] reveal the piezoelectric character of the PNDs. These resonances are macroscopic manifestations of a relatively strong TO-TA coupling mediated by the PNDs. Here, we have shown that this interaction also involves the LMs associated with the tunneling of the off-center Nb.

The results presented here should be useful for the study of other relaxor ferroelectrics with homovalent cations KLT, BZT, and BST in which strong random fields are absent. In the lead relaxors PMN and PZN, the heterovalent substituted ions give rise to REFs that should be somewhat screened by the off-center ions and may also partially suppress the tunneling motion of the Nb ions within individual unit cells.

### V. CONCLUSION

In the present paper, we have reported measurements of the TA and TO phonon in KTN crystals with Nb concentrations of 15% and 17%. In addition to the TO and TA phonons, these results suggest the existence of LM that can be associated with the collective or cooperative tunneling reorientation of the off-center  $\text{Nb}^{5+}$  ions mediated by the TO phonon. These LM modes are strongly coupled with the TO phonon and interact with the TA, giving rise to increased damping for intermediate values of the wavevector,  $q \geq 0.07$ , which correspond approximately to the size of the PNDs. Transitions between  $\text{Nb}^{5+}$  tunneling states that would otherwise not be excited by the TA



phonon become allowed with the appearance of the quasistatic polarization of PNRs or static polarization of PNDs. The TO-LM coupling also qualitatively explains the incomplete softening of the TO mode. Conversely, it is the displacements of the same Nb ions correlated through the TO field that give rise to the formation of these PNRs and PNDs. Therefore, the same Nb ions take part simultaneously in both the relatively high frequency TO motion and the relatively slow off-center or pseudospin correlated motion, i.e., a two-time scale dynamics [30]. At high temperature, the TO mode-driven Nb dynamics and the Nb off-center pseudospin dynamics are almost independent from each other because of their large difference in frequency or time scales, and the displacements of different off-center Nb ions are mostly uncorrelated. Upon cooling, the evolution of the system can be described as follows. (i) The pseudo spin-pseudospin interaction strengthens, and the displacements of the off-center Nb ions become correlated giving rise to a LM. (ii) The dynamics of the TO and pseudospin becomes mixed, and a coupled TO-pseudospin LM mode appears. (iii) This mixed LM mode eventually condenses, resulting in the appearance of static atomic displacements and local polarization  $P$  within regions or droplets (PNDs), local strain fields, the relaxor behavior of the dielectric susceptibility, and the dielectric resonances mentioned earlier [14,29,30]. The TA phonon damping reaches a maximum at  $\sim 136$  K [Figs. 6(b) and 10(b)] due to the increasing number of PNDs. At low temperature, the coupling between the TO mode and the off-center Nb pseudospin dynamics weakens because the reorientation frequency of the off-center Nb falls away from the increasing soft mode frequency and the crystal returns to a regime similar to that of ordinary ferroelectrics. In such a scenario, the THz frequency TA phonon excited by neutrons acts as a probe of the TO-Nb<sup>+5</sup> dynamics in KTN.

#### ACKNOWLEDGMENTS

Special thanks to L. A. Boatner for the KTN crystals and to P. Gehring for useful discussions. The experimental part of this paper was initially supported by the U S Department of Energy under Grant No. DE-FG-06ER46318.

#### APPENDIX A

##### The HN relaxation model

The HN relaxation [11,17,18] is an empirical modification of the Debye relaxation model that takes into account the asymmetry and breadth of the dielectric dispersion curve by adding two exponential parameters  $\alpha$  and  $\beta$  to the Debye [Eqs. (6)–(8)]. The asymmetry and breadth of the corresponding spectra are described by the parameters  $\alpha$  and  $\beta$ . The Debye relaxation correspond to the case  $\alpha = 1, \beta = 1$ .

The HN model can be described as a superposition of Debye models with a continuous distribution  $g(\ln \tau_D)$  of the relaxation time,  $\tau_D$ :

$$\frac{\chi(\omega|\alpha, \beta) - \chi_\infty}{\Delta\chi} = \int_{\tau_D=0}^{\infty} \frac{1}{1 + i\omega\tau_D} g(\ln \tau_D) d \ln \tau_D$$

$$g(\ln \tau_D|\alpha, \beta) = \frac{1}{\pi} \frac{(\tau_D/\tau)^{\alpha\beta} \sin(\beta\theta)}{((\tau_D/\tau)^{2\alpha} + 2(\tau_D/\tau)^\alpha \cos(\pi\alpha) + 1)^{\beta/2}},$$

$$\theta = \arctan \left( \frac{\sin(\pi\alpha)}{(\tau_D/\tau)^\alpha + \cos(\pi\alpha)} \right)$$

if the argument of the arctangent  
is positive, otherwise

$$\theta = \arctan \left( \frac{\sin(\pi\alpha)}{(\tau_D/\tau)^\alpha + \cos(\pi\alpha)} \right) + \pi. \quad (\text{A1})$$

The HN model with  $0 < \alpha < 1$  and  $\beta = 1$  is often used to describe the so-called stretched relaxations of polymers and glasses. By contrast, our experimental results are satisfactorily fitted in the framework of the HN model with values  $\alpha \approx 3/2 \div 1.7$  (i.e., greater than 1) and  $\beta = 1$ . The HN relaxation model in Eq. (6) must satisfy general analytical conditions (causality) in the complex frequency plane  $\omega$  [31]. In the case of  $\alpha = 3/2$  and  $\beta = 1$ , the HN function and the distribution function (A1) have a branch point at  $\omega = 0, \tau_D = 0$ . The requirement of causality [31] will be satisfied if we make corresponding cuts in the line connecting two Riemann surfaces in the complex  $\omega$  and  $\tau_D$  planes. In this case, it is therefore difficult to interpret the function (A1) directly as due to a distribution of relaxation times in this case.

Instead, let us consider the HN relaxation function  $F_{\text{HN}}(t)$  in the time-domain representation:

$$F_{\text{HN}}(t|\alpha = 3/2, \beta = 1) = \int_{-\infty}^{\infty} \frac{\exp(i\omega t)}{1 + (i\omega\tau)^{3/2}} d\omega, \quad (\text{A2})$$

$$F_{\text{HN}}(t < 0|\alpha = 3/2, \beta = 1) = 0$$

Expression (A2) is used in the numerical calculation of the HN relaxation function shown in Fig. 12.

The function  $F_{\text{HN}}(t > 0|\alpha = 3/2, \beta = 1)$  can also be calculated by integration in the complex  $\omega$  plane with cuts along the imaginary semi-axis from  $+0$  to  $+i\infty$ . We then have

$$F_{\text{HN}}(t > 0|\alpha = 3/2, \beta = 1)$$

$$= -S + \frac{8\pi}{3\tau} \exp\left(-\frac{t}{2\tau}\right) \cos\left(\frac{t}{\tau} \frac{\sqrt{3}}{2} - \frac{\pi}{3}\right),$$

with  $S(t) = \frac{2}{t} \int_0^{\infty} \frac{(w\tau/t)^{3/2}}{(1 + (w\tau/t)^3)} \exp(-w) dw$

in which  $w$  is simply the variable of integration  
and  $S(t \gg \tau)$

$$\approx \frac{2\tau^{3/2}}{t^{5/2}} \times \sum_{n=0}^{\infty} (-1)^n \Gamma(3n + 5/2)! (\tau/t)^{3n}. \quad (\text{A3})$$

The pole term (A3)  $\sim \exp(-\frac{t}{2\tau}) \cos(\frac{t}{\tau} \frac{\sqrt{3}}{2} - \frac{\pi}{3})$  corresponds to a resonance at the frequency  $\omega_p = \sqrt{(3/2)/\tau}$ . The parameters of this pole term (frequency, rate of decay) are in an agreement with those obtained from the Lorentzian fit in Fig. 12.

#### APPENDIX B

Model of the tunneling transitions of the Nb off-center ion between (111) positions.

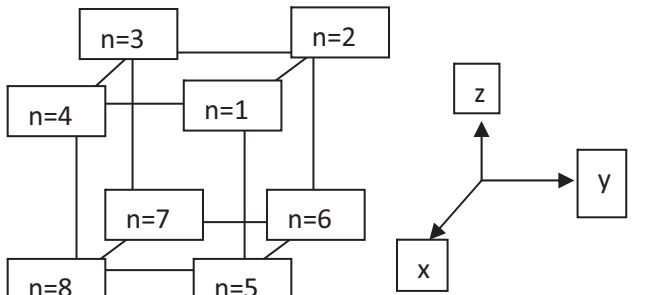
We consider tunneling transitions of one Nb ion between (111) type positions in the cubic unit cell. The Nb ion can occupy any one of the eight sites at the corners of the unit



cell with coordinates  $x = \pm 1$ ,  $y = \pm 1$ ,  $z = \pm 1$ . These are numbered as  $n = 1-8$ . Their positions can be described by the  $(8 \times 3)$  matrix  $S$ :

$$\begin{aligned} S[n = 1, x, y, z] &= 1, 1, 1; S[n = 2, \dots] = -1, 1, 1; S[n = 3, \dots] \\ &= -1, -1, 1; S[n = 4, \dots] = 1, -1, 1; \\ S[n = 5, \dots] &= 1, 1, -1; S[n = 6, \dots] \\ &= -1, 1, -1; S[n = 7, \dots] = -1, -1, -1; \\ S[n = 8, \dots] &= 1, -1, -1. \end{aligned} \quad (\text{B1})$$

For simplicity, we take into account tunneling only along cubic edges, i.e., between nearest (111) type positions, with frequency  $\Omega$ . The tunneling Hamiltonian  $H_T$  is written as an  $8 \times 8$  matrix with corresponding eigenvectors  $E(m)$  and orthogonal eigenfunctions  $\psi(m)$  in the representation (B1):



$$H_T = -\Omega \begin{pmatrix} 0 & 1 & 0 & 1 & 1 & 0 & 0 & 0 \\ 1 & 0 & 1 & 0 & 0 & 1 & 0 & 0 \\ 0 & 1 & 0 & 1 & 0 & 0 & 1 & 0 \\ 1 & 0 & 1 & 0 & 0 & 0 & 0 & 1 \\ 1 & 0 & 0 & 0 & 0 & 1 & 0 & 1 \\ 0 & 1 & 0 & 0 & 1 & 0 & 1 & 0 \\ 0 & 0 & 1 & 0 & 0 & 1 & 0 & 1 \\ 0 & 0 & 0 & 1 & 1 & 0 & 1 & 0 \end{pmatrix}. \quad (\text{B2})$$

The ground state energy is  $E = \langle \psi_s | H | \psi_s \rangle = -3\Omega$  and corresponds to a fully symmetric wave function  $\psi_s = [1, 1, 1, 1, 1, 1, 1, 1]$ . Wave functions corresponding to excited states are obtained by means of the commuting operators  $X$ ,  $Y$ ,  $Z$ :

$$\begin{aligned} X &= \sum_{j=1}^8 X^{(j)}, \quad Y = \sum_{j=1}^8 Y^{(j)}, \quad Z = \sum_{j=1}^8 Z^{(j)}, \\ XY &= YX, \quad XZ = ZX, \quad YZ = ZY, \quad X^2 = Y^2 = Z^2 \sim 1. \end{aligned} \quad (\text{B3})$$

For example,  $XS[n = 1, x = 1, y = 1, z = 1] \sim +S[n = 1]$ ,  $XS[n = 2, x = -1, y = 1, z = 1] \sim -S[n = 2]$ , ..., where we omit factor normalization.

The excited states are the triplet  $X\psi_s, Y\psi_s, Z\psi_s$  with  $E = -\Omega$ , the triplet  $XY\psi_s, YZ\psi_s, ZX\psi_s$  with  $E = +\Omega$ , and the singlet  $XYZ\psi_s$  with  $E = +3\Omega$ . The dipole operators,  $X, Y, Z$ , excite transitions with energy  $\pm 2\Omega$ ; quadrupole operators,  $XY, XZ, YZ$ , excite transitions with energy  $\pm 4\Omega$  and *elastic* transitions within the triplet manifolds  $X\psi_s, Y\psi_s, Z\psi_s$  and  $XY\psi_s, YZ\psi_s, ZX\psi_s$ ; and the octupole operator,  $XYZ$ , excites transitions with energy  $\pm 2\Omega, \pm 6\Omega$ .

The  $\text{Nb}^{+5}$  ions are displaced from their high symmetry positions by a relatively small  $R_{\text{Nb}} = 0.145 \text{ \AA}$  in (111) directions,

and we express the values of the matrix elements in terms of the small dimensionless parameter  $r_{\text{Nb}} \equiv R_{\text{Nb}}/1. \text{u.} = 0.036 \ll 1$ ;  $X, Y, Z \sim r_{\text{Nb}}$ ;  $XY, YZ, ZX \sim r_{\text{Nb}}^2$ ;  $XYZ \sim r_{\text{Nb}}^3$ .

The Hamiltonian terms describing the TO and TA phonon interaction with the tunneling ions will be different for SR and so-called LR forces, which include polarization. For simplicity, we do not take into account the modulation of the potential barrier caused by the TO and TA phonons.

### 1. The TO, Short Range (SR)

The  $R^{(i)}$  designates the eight polar vector operators,  $\xi$  the TO displacement, and  $n$  is a unit vector directed along the TO momentum  $q$ . The corresponding interaction  $V(\text{TO}|\text{SR})$  can be written as follows:

$$\begin{aligned} V(\text{TO}|\text{SR}) &\equiv V^{(1)}(\text{TO}|\text{SR}) + V^{(2)}(\text{TO}|\text{SR}), \\ V^{(1)}(\text{TO}|\text{SR}) &= A(\text{TO}|\text{dip})[n \times \xi] \sum_{i=1}^8 [n \times R^{(i)}] \propto (r_{\text{Nb}}), \\ V^{(2)}(\text{TO}|\text{SR}) &= A(\text{TO}|\text{quad}) \\ &\times \sum_{i,j=1}^8 (R^{(i)} R^{(j)})_{\alpha\beta} (q\xi)_{\alpha\beta} \propto q(r_{\text{Nb}})^2, \\ (q\xi)_{\alpha,\beta} &\equiv 1/2(q_\alpha \xi_\beta + q_\beta \xi_\alpha - 2/3 \delta_{\alpha\beta} (q\xi)), \\ (R^{(i)} R^{(j)})_{\alpha,\beta} &\equiv 1/2(R^{(i)}_\alpha R^{(j)}_\beta + R^{(i)}_\beta R^{(j)}_\alpha \\ &- 2/3 \delta_{\alpha\beta} (R^{(i)} R^{(j)})). \end{aligned} \quad (\text{B4})$$

The  $A(\text{TO}|\text{dip})$  and  $A(\text{TO}|\text{quad})$  are constants of interaction. The term  $V^{(1)}(\text{TO}|\text{SR})$  describes dipole transitions with  $\Delta E = \pm 2\Omega$ . The  $V^{(2)}(\text{TO}|\text{SR})$  excites transitions with energy  $\Delta E = \pm 4\Omega$  and *elastic* transitions within the triplets  $X\psi_s, Y\psi_s, Z\psi_s$ , and  $XY\psi_s, YZ\psi_s, ZX\psi_s$ . We should note that the  $V^{(1)}(\text{TO}|\text{SR})$  dipolar interaction is much stronger than the quadrupolar one,  $V^{(2)}(\text{TO}|\text{SR})$ .

### 2. TO, weak octupole transition

$$\begin{aligned} V(\text{TO}|\text{octo}) &\equiv A(\text{TO}|\text{octo}) \sum_{i,j,k=1}^8 (qR^{(i)})(qR^{(j)})(R^{(k)}\xi) \\ &\propto q^2 (r_{\text{Nb}})^3, \end{aligned} \quad (\text{B5})$$

in which  $A(\text{TO}|\text{octo})$  is the constant of the interaction.  $V(\text{TO}|\text{octo})$  interaction could excite octuplet transitions with  $\Delta E = \pm 6\Omega$  and dipole transitions with  $\Delta E = \pm 2\Omega$ .

### 3. The TA, SR

The  $V(\text{TA}|\text{SR})$  can be written as follows [32]:

$$V(\text{TA}|\text{SR}) = - \sum_{i=1}^8 w_{\alpha\beta}^{(i)} \sigma_{\alpha\beta}, \quad (\text{B6})$$

where  $\sigma_{\alpha\beta}$  is the stress tensor and  $w_{\alpha\beta}^{(i)}$  the elastic dipole *tensor* corresponding to the  $i$ th (111) type cubic corner. The value of  $w_{\alpha\beta}^{(i)}$  is defined by the geometry of the potential well. Let's suppose that  $\lambda_L$  and  $\lambda_P$  are the main values of the tensor  $w_{\alpha\beta}^{(i)}$

in the coordinate system with  $z$  axis along a (111) direction. We then obtain in the coordinate system (100), (010), (001):

$$\sum_{i=1}^8 w^{(i)} \sim \frac{2}{3}(\lambda_L - \lambda_P)(XY + YZ + ZX) \propto (r_{\text{Nb}})^2. \quad (\text{B7})$$

Therefore, the interaction of the *elastic* dipole with the stress generated by the TAW leads to quadrupolar transitions,  $\Delta E = \pm 4\Omega$ , and elastic transitions,  $\Delta E = 0$ , connecting states *inside* the triplets with energy  $E = -\Omega$  and  $E = +\Omega$ .

#### 4. The TA, long range (LR)

Assuming that the electric field  $E$  generated by the TA phonon and interacting with the electric dipole moment appears due to the displacement of the  $\text{Nb}^{+5}$  ion from its high symmetry position, the interaction term,  $V(\text{TA}|\text{LR})$ , can be written

$$\begin{aligned} V(\text{TA}|\text{LR}) &= A_{\text{TA}} \sum_{i=1}^8 (R^{(i)}P)_{\alpha\beta} \tilde{u}_{\alpha\beta}, \\ \tilde{u}_{\alpha\beta} &\equiv 1/2(u_{\alpha}q_{\beta} + u_{\beta}q_{\alpha} - 2/3\delta_{\alpha\beta}(\mathbf{u}\mathbf{q})) \\ (R^{(i)}P) &\equiv 1/2(R^{(i)}_{\alpha}P_{\beta} + R^{(i)}_{\beta}P_{\alpha} - 2/3\delta_{\alpha\beta}(\mathbf{R}^{(i)}\mathbf{P})), \\ \mathbf{R}^{(i)}_{\mathbf{x}} &= \mathbf{X}^{(i)}, \dots \end{aligned} \quad (\text{B8})$$

Here  $A_{\text{TA}}$  is the constant of interaction, and  $P$  is the polarization vector. Such polarization arises due the atomic displacements that accompany the formation of the quasistatic PNRs or static PNDs. The physical meaning of (B8) can be explained as follows. Let's suppose that the polarization  $P$  is directed along the  $z$  axis. This perturbation creates a correction to the wave functions  $\psi_S$  and  $X\psi_S$ :

$$\delta\psi_S = -\frac{P}{2\Omega}Z\psi_S, \quad \delta X\psi_S = -\frac{P}{2\Omega}ZX\psi_S. \quad (\text{B9})$$

The elastic dipole-stress interaction (B7) and (B8) then leads to the existence of the nonzero matrix element between  $\psi_S$  and  $X\psi_S$ :

$$\begin{aligned} &\langle \psi_S + \delta\psi_S | V(\text{TA}|\text{SR}) | X\psi_S + \delta X\psi_S \rangle \\ &\sim \frac{P}{\Omega}(\lambda_L - \lambda_P)\sigma_{x,z}, \quad \Delta E = \pm 2\Omega. \end{aligned} \quad (\text{B10})$$

Therefore, the appearance of the polarization  $P$  opens transitions  $\Delta E = \pm 2\Omega$  that are otherwise forbidden when

$P = 0$ . This is quite consistent with the ultrasonic results obtained by Knauss *et al.*, which evidenced the coupling between a transverse ultrasonic wave and the tunneling Nb ions in the presence of the PNDs [16].

In the case of strong polarization, when  $P \gg \Omega$ , the wave function will be restricted to a subset of four corners of the cubic unit cell, corresponding to tetragonal symmetry. If restricted, for instance, to the plane  $z = 1$ , the wave function components  $S_P$  will then be

$$S_P = [[1, 1], [-1, 1], [-1, -1], [1, -1]]. \quad (\text{B11})$$

The tunneling Hamiltonian  $H_{\text{TP}}$  and the corresponding eigenvalues and eigenvectors in the representation (B11) can be written as follows:

$$\begin{aligned} H_{\text{TP}} &= -\Omega \begin{bmatrix} 0, & 1, & 0, & 1 \\ 1, & 0, & 1, & 0 \\ 0, & 1, & 0, & 1 \\ 1, & 0, & 1, & 0 \end{bmatrix} \\ \Psi_{PS} &= [1, 1, 1, 1], \quad E_{PS} = -2\Omega, \\ \Psi_{PXmY} &= ((X - Y)/2)\Psi_{PS} = [0, -1, 0, 1], \quad E_{PXmY} = 0, \\ \Psi_{PXpY} &= ((X + Y)/2)\Psi_{PS} = [1, 0, -1, 0], \quad E_{PXpY} = 0, \\ \Psi_{PXY} &= XY\Psi_{PS} = [1, -1, 1, -1], \quad E_{PXY} = +2\Omega \end{aligned} \quad (\text{B12})$$

The elastic dipole-stress interaction in (B6) and (B7) leads to the existence of nonzero matrix elements corresponding to the inelastic and elastic transitions,  $\Delta E = \pm 2\Omega$  and  $\Delta E = 0$ , between states (B12) for the case of the TAW propagating along the  $z$  axis. Transitions corresponding to  $\Delta E = \pm 4\Omega$  could also be excited for a TAW propagating and polarized in the  $x$ - $y$  plane. We should note that the effect of the phonon polarization depends on the direction of the electric polarization  $P$ . As an example, for a strong polarization  $P$  along the (111) axis, the wave function will be locked at the cubic (111) corner, and tunneling of the Nb off-centers and its effect on the damping of the TA phonon will be suppressed. Finally, it is worth mentioning that the calculations corresponding to (B8)–(B12) are similar to those used to describe the features of a ferroelectric crystal placed in a symmetry-breaking field.

- 
- [1] P. M. Gehring, *J. Adv. Dielectrics* **02**, 1241005 (2012); D. Phelan, C. Stock, J. A. Rodriguez-Rivera, S. Chi, J. Leao, X. Long, Y. Xie, A. A. Bokov, Z.-G. Ye, P. Ganesh, and P. Gehring, *Proc. Nat. Acad. Sci. U.S.A.* **111**, 1754 (2014); R. A. Cowley, S. N. Gvasalija, S. G. Lushnikov, B. Roesli, and G. M. Rotaru, *Adv. Phys.* **60**, 229 (2011).
- [2] J. Toulouse, *Ferroelectrics* **369**, 203 (2008); J. Toulouse, F. Jiang, O. Svitelskiy, W. Chen, and Z.-G. Ye, *Phys. Rev. B* **72**, 184106 (2005). Note that in the 2005 paper, Burns temperature and the intermediate temperature at which the PNDs form were labeled  $T_B$  and  $T_d$ , respectively, but as  $T_B$  and  $T^*$  in the 2008 paper.
- [3] M. E. Manley, J. W. Lynn, D. L. Abernathy, E. D. Specht, O. Delaire, A. R. Bishop, R. Sahul, and J. D. Budai, *Nat. Commun.* **5**, 3683 (2014).
- [4] P. M. Gehring, D. Parshall, C. Stock, G. Xu, X. Li, and H. Luo, *Fundamental Physics of Ferroelectrics and Related Materials 2016*, Washington, DC, January 31–February 3, 2016. Book of Extended Abstracts, [https://ferro2016.carnegiescience.edu/sites/default/files/Ferro\\_2016\\_Abstract\\_Book.pdf](https://ferro2016.carnegiescience.edu/sites/default/files/Ferro_2016_Abstract_Book.pdf).
- [5] K. Hirota, Z. G. Ye, S. Wakimoto, P. M. Gehring, and G. Shirane, *Phys. Rev. B* **65**, 104105 (2002).

- [6] C. Stock, H. Luo, D. Viehland, J. F. Li, I. P. Swainson, R. J. Birgeneau, and G. Shirane, *J. Phys. Soc. Jpn.* **74**, 3002 (2005).
- [7] C. Stock, P. M. Gehring, H. Hiraka, I. Swainson, G.-G. Xu, Z.-G. Ye, H. Luo, J.-F. Li, and D. Viehland, *Phys. Rev. B* **86**, 104108 (2012).
- [8] G. Yong, R. Erwin, O. Svitelskiy, J. Toulouse, L. Boatner, B. Hennion, S. Shapiro, APS March Meeting D10, 002 (2009), <http://meetings.aps.org/link/BAPS.2009.MAR.D10.2>.
- [9] O. Hanske-Petitpierre, Y. Yacoby, J. Mustre de Leon, E. A. Stern, and J. J. Rehr, *Phys. Rev. B* **44**, 6700 (1999).
- [10] Y. Girshberg and Y. Yacoby, *Solid State Commun.* **103**, 425 (1997); Y. Yacoby and Ya. Girshberg, Phase Transitions in Perovskites with Off-center Ion Displacements, <https://www.gl.ciw.edu/static/users/./Yacoby.pdf>.
- [11] S. Havriliak and S. Negami, *Polymer* **8**, 161 (1967).
- [12] J. Toulouse, E. Iolin, B. Hennion, D. Petitgrand, G. Yong, and R. Erwin, [arXiv:1001.4096](https://arxiv.org/abs/1001.4096) (2010).
- [13] E. Iolin, J. Toulouse, B. Hennion, D. Petitgrand, and R. Erwin, Fundamental Physics of Ferroelectrics and Related Materials 2016, Washington, DC, January 31–February 3, 2016. Book of Extended Abstracts, [https://ferro2016.carnegiescience.edu/sites/default/files/Ferro\\_2016\\_Abstract\\_Book.pdf](https://ferro2016.carnegiescience.edu/sites/default/files/Ferro_2016_Abstract_Book.pdf).
- [14] R. K. Pattnaik and J. Toulouse, *Phys. Rev. Lett.* **79**, 4677 (1997).
- [15] E. Iolin, J. Toulouse, and R. Erwin, Neutron Scattering Study of the Phase Transition in the Mixed Ferroelectric Single Crystal  $\text{Ta}_{0.83}\text{Nb}_{0.17}\text{O}_3$ , Fundamental Physics of Ferroelectrics 2007, Colonial Williamsburg, VA, February 11–14, 2007. Book of Extended Abstracts; G. Shirane, S. Shapiro, and J. Tranquada, *Neutron Scattering with a Triple-Axis Spectrometer* (Cambridge University Press, Cambridge, 2002), §2.4, p. 28.
- [16] J. D. Axe, J. Harada, and G. Shirane, *Phys. Rev. B* **1**, 1227 (1970); L. A. Knauss, X. M. Wang, and J. Toulouse, *ibid.* **52**, 13261 (1995).
- [17] R. Zorn, *J. Polym. Sci., Part B* **37**, 1043 (1999).
- [18] R. Hilfer, *J. Non-Cryst. Solids* **305**, 122 (2002).
- [19] M. A. Isakovich and I. A. Chaban, *Zh. Eksp. Teor. Fiz. (USSR)* **50**, 1343 (1966) [*Sov. Phys. JETP* **23**, 893 (1966)]; See also, Jeppe C. Dyre, *Phys. Rev. E* **72**, 011501 (2005).
- [20] S. M. Shapiro, J. D. Axe, G. Shirane, and T. Riste, *Phys. Rev. B* **6**, 4332 (1972).
- [21] B. I. Halperin and C. M. Varma, *Phys. Rev. B* **14**, 4030 (1976).
- [22] P. C. Hohenberg and B. I. Halperin, *Rev. Mod. Phys.* **49**, 435 (1977).
- [23] A. D. Bruce and R. A. Cowley, *Structural Phase Transitions, Part III* (Taylor & Francis, London, 1981).
- [24] R. M. Lynden-Bell and K. H. Michel, *Rev. Mod. Phys.* **66**, 721 (1994).
- [25] K. H. Michel and J. J. Naudts, *J. Chem. Phys.* **68**, 216 (1978).
- [26] Y. Girshberg and Y. Yacoby, *J. Phys.: Condens. Matter* **24**, 015901 (2012).
- [27] V. G. Vaks, *Introduction to the Microscopic Theory of Ferroelectrics* (in Russian) (Nauka, Moscow, 1973).
- [28] E. Iolin, Inelastic and Quasi Elastic Neutron Scattering by the Depolarizing Soft Mode in Relaxor, Fundamental Physics of Ferroelectrics 2014, Carnegie Institution of Washington, Washington, DC, January 26–29, 2014. Book of Extended Abstracts.
- [29] J. Toulouse, Nanoscale Structure and the Two-Timescale Dynamics of Relaxor Ferroelectrics, <http://meetings.aps.org/link/BAPS.2005.MAR.W5.4>.
- [30] J. Toulouse, L. Cai, R. K. Pattnaik, and L. A. Boatner, *Europhys. Lett.* **105**, 17001 (2014).
- [31] L. D. Landau and E. M. Lifshitz, *Electrodynamics of Continuous Media* (FizMatLit, Moscow, 1959), Chap. IX, p. 62.
- [32] U. H. Kopvillem and P. V. Saburova, *Paraelectric Resonance* (Nauka, Moscow, 1982), Chap. 2 and 4 (in Russian).